Paleomagnetism, paleointensity and geochronology of a Proterozoic dolerite dyke from southern West Greenland

Miki, Masako ; Seki, Hanae ; Yamamoto, Yuhji ; Gouzu, Chitaro ; Hyodo, Hironobu ; Uno, Koji ; Otofuji, Yo-ichiro

(Citation)
Journal of Geodynamics, 139:101752

(Issue Date)
2020-09

(Resource Type)
journal article

(Version)
Accepted Manuscript

Paleomagnetism, Paleointensity and Geochronology of a Proterozoic dolerite dyke from southern West Greenland

Masako MIKI[1], Hanae SEKI[1], Yuhji YAMAMOTO[2], Chitaro GOUZU[3], Hironobu HYODO[4], Koji UNO[5] and Yo-ichiro OTOFUJI[6]

1: Department of Planetology, Graduate School of Science, Kobe University, Kobe 657-8501, Japan

2: Center for Advanced Marine Core Research, Kochi University, Kochi 783-8502, Japan

3: Hiruzen Institute for Geology and Chronology, 2-5 Nakashima, Naka-ku, Okayama 703-8252, Japan

4: Research Institute of Natural Sciences, Okayama University of Science, 1-1 Ridai-cho, Okayama 700-0005, Japan

5: Faculty of Education, Okayama University, Okayama, Japan

6: Institute of GeoHistory, Susai 1599, Akaiwa, Okayama 701-2503, Japan

Corresponding author

Masako Miki

Phone 81-78-803-6535

E-mail makomiki@kobe-u.ac.jp

Abstract

Archean to Paleoproterozoic rocks potentially record the evolution of the geodynamo and the tectonic mode of the early Earth. The paleomagnetic intensity and direction data provide important information on the Earth's core–mantle revolution. Herein, we report the results of paleomagnetic and geochronological studies of a Proterozoic dolerite dyke from southern West Greenland. Clinopyroxene grains from the dyke yielded Ar–Ar plateau ages from 1,808 to 1,887 Ma (1,816.0 ± 14.6 Ma; 2σ). The paleomagnetic direction of the dyke (D = 243.6°, I = 66.3°, α_{95} = 3.9°) yielded a virtual geomagnetic pole (VGP) of 33.5°N and 96.4°W. This 1.8 Ga pole falls in a limited area where Paleoproterozoic poles between 2.5 Ga and 1.7 Ga for southern West Greenland are distributed. Comparison of the Paleoproterozoic poles of southern West Greenland with those of North America suggests that the North Atlantic Craton of southern Greenland could have been an independent stagnant tectonic block, different from the drifting Superior and Slave Cratons in the Early Proterozoic. Thellier experiments on 13 specimens yielded a mean paleointensity value of 14.8 ± 2.3 μT, indicating a virtual dipole moment of 2.88 ± 0.46 × 10^{22} Am^2. This value is approximately one-third of the present-day Earth's field intensity, and is consistent with the value for the period between 1,400 Ma and 2,400 Ma. This small paleointensity value of the Proterozoic rocks is due to a gradual dipole moment change over a long period (~1 Gyrs) since 4,000 Ma.

Key words

North Atlantic craton

Greenland

geochronology

paleomagnetic pole

paleointensity

Proterozoic

1. INTRODUCTION

During the Archean to Proterozoic, the Earth's interior state should have greatly changed due to long-term cooling of the early Earth. The Earth has experienced solid inner core nucleation in the molten core and the evolution of plate tectonics as a result of the changes in the mantle convection state. The Precambrian paleomagnetic data (field strength and direction) shed light on such an evolution. In this paper, we report reliable paleomagnetic data of the Proterozoic rocks from southwestern Greenland in order to add to the knowledge of early Earth’s evolution.

The first interest regarding Precambrian paleomagnetism is the variation of geomagnetic paleointensity during the core–mantle evolution. The biggest event in this evolution was the inner core nucleation. A sudden increase in the Mesoproterozoic geomagnetic field intensity due to the inner core nucleation has been suggested from the PINT database (Biggin et al., 2015). Alternatively, some recent studies (Smirnov et al., 2016; Kodama et al., 2019; Bono et al., 2019) pointed out the possibility of inner core nucleation during the Phanerozoic Era. Prior to the nucleation, the Proterozoic geomagnetic field should have been generated by long-term cooling without any compositional convection in the outer core due to inner core growth, as seen in the present Earth’s interior. The mechanism for the Proterozoic geomagnetic field is an unresolved issue, although convection in the liquid core (Hirose et al., 2017) or the lowermost mantle (Ziegler and Stegman, 2013) is considered. The paleointensity data are important information to establish the robust aspect of long-term variation in the geomagnetic field.

Another interesting issue is a dispute about when and how modern-style plate tectonics began (Stern, 2008; Hamilton, 2011; Korenaga, 2013; Condie, 2018). The onset of plate tectonics is intrinsically connected with the mantle state and the thermal history of the early Earth. In a mantle convection simulation, O'Neil et al., (2016) suggested that the Earth may have begun in a hot stagnant lid mode, evolving into an episodic regime, before finally passing into a plate tectonic regime. A paleomagnetic study of Archean to Paleoproterozoic rocks provides a clue to the tectonic evolution of the Earth because the relative movement of the continents should be recorded in the paleomagnetic directional data.

Our paleomagnetic study focuses on southern West Greenland in the North Atlantic Craton. The Superior and Slave Cratons are its neighbors (Fig. 1). Their apparent polar wandering paths (APWPs) suggest that the Superior and Slave Cratons have moved independently of the plate tectonic manner in the Paleoproterozoic era (Mitchell et al., 2014; Buchan et al., 2016) and that by 2.0–1.7 Ga, the two cratons gathered to form the

Laurentia, the core of the Paleo-to-Mesoproterozoic super continent Nuna (e.g. Hoffman 1997). We attempt to construct the Paleoproterozoic APWP for southern Greenland of the North Atlantic Craton, although the amount of data is scarce. Its APWP can detect the tectonic motion of the North Atlantic Craton. The comparison of APWPs for three cratons, the North Atlantic, Superior, and Slave Cratons, can test a formation aspect of the first supercontinent Nuna.

Several generations of Paleoproterozoic mafic dykes were emplaced in the Archean block of southern West Greenland (e.g. Hall and Hughes, 1990). Paleomagnetic studies of these Paleoproterozoic dykes have provided reliable Paleoproterozoic data of paleointensity and direction (Morimoto et al., 1997; Miki et al., 2009). We focus again on the dykes to accumulate paleomagnetic information concerning geomagnetic field intensity and tectonic movements of southern Greenland and of the North Atlantic Craton in Paleoproterozoic time.

We chose a NE-trending dolerite dyke close to Nuuk town (64.36°N, 51.33°W) in the Archean craton. Because the trend of a dyke is not always a reliable index to its intruding age in southern Greenland (Nilsson et al., 2013), $^{40}Ar/^{39}Ar$ dating was applied to the rock samples first. Then, a paleomagnetic pole for the dyke was compared with the contemporaneous paleomagnetic poles from southern Greenland. This paper is the first contribution on the evolution of Proterozoic global tectonics based on paleomagnetic directions from southern Greenland.

2. GEOLOGY AND SAMPLING

The Archean craton of southern Greenland (Fig. 2) consists mainly of Eoarchean to Neoarchean (ca. 3.8–2.7 Ga) metamorphosed tonalite–trondhjemite–granodiorite suites (TTGs), amphibolite-dominant greenstone belts, and layered anorthosite complexes (Friend and Nutman, 2005; Windley and Garde, 2009; Polat et al., 2011). Paleoproterozoic mafic dyke swarms are recognized throughout the western area of the Archean craton. The dyke swarms south of Nuuk are named MD dykes. Although these dykes have been previously collectively named metadolerite (MD) dyke swarms (Bridgewater et al., 1976) in the area where they were first mapped, no metamorphism or alteration has been observed in other areas. Many of the dykes are 20–50 m wide and extend for several tens of kilometers. The dykes are almost all vertical or nearly vertical and chilled contacts with the host Archaean gneiss are commonly preserved.

Three periods of emplacement, represented by MD1, MD2, and MD3, are approximately distinguishable by their characteristic orientations (Hall and Hughes, 1987; 1990). The youngest SE-NW to E-W MD3 dykes yield U-Pb ages between 2,030 and 2,050 Ma (Nilsson et al., 2010; 2013), and they are coeval with the Kangamiut dykes. For an NE-SW–trending dyke (MD2), Nilsson et al. (2013) reported a baddeleyite U-Pb age of 2,209 ± 5 Ma (2σ). The oldest MD1 dyke seems to include two age groups (Nilsson et al., 2013); the N-S–trending ~2.5 Ga Kilaarsarfik dykes and the 2.37 Ga E-W–trending Grædefijord dykes. A similar Ar–Ar age (2,585 Ma) for the Kilaarsarfik dyke was reported from an E-W–trending dyke in Nuuk area (Miki et al., 2009), although a U-Pb baddeleyite age of 2,125 ± 9 Ma (2σ) was reported from the same sample (Nilsson et al., 2019).

The Archean craton in Greenland is bounded by the ENE-striking Paleoproterozoic Nagssugtoqidian Orogen in the north (Fig. 2). The orogen is 300 km wide and subdivided into three tectonic segments: The Northern, Central, and Southern Nagssugtoqidian Orogen (NNO, CNO, and SNO respectively; Marker et al., 1995). High-grade metamorphism occurred in the CNO around 1,850 Ma, during the collision event of Archean terrains (Connely et al., 2000; Kalsbeek et al., 1984, 1987; Kalsbeek and Nutman 1996; Tayler and Kalsbeek 1990) followed by very slow cooling (Willigers et al., 1999, 2001, 2002). To the south, the grade of metamorphism decreases to amphibolite facies in the SNO (e.g. Connelly et al., 2000). Paleoproterozoic mafic dykes (Kangamiut dykes) also intrude in the SNO and the southern Nagssugtoqidian foreland.

The dykes are undeformed in the southern Nagssugtoqidian foreland and progressively more deformed northward.

We collected samples from an NE-trending small dolerite dyke that is 3.4 m wide (Fig. 2) and located 10 km north of Nuuk town. Although most of the intrusions in this area are non-metamorphosed MD dykes, the geochronological results in this study indicate that the collected intrusion is not an MD dyke but rather of a younger generation. Fifteen oriented block samples from the eastern chilled margin (named site GP72) and nine samples from the western margin (site GP75) were taken with both sun and magnetic compasses. The bedding attitude is probably flat because the dyke intrudes vertically. Samples for geochronological study were also collected.

To conduct a baked contact test, samples were collected from the host gneiss at one locality near the eastern margin (site GP71, 10 to 20 m from the contact) and three different localities near the western margin (site GP 76, contact; site GP74, ~30 cm from the contact; site GP73, ~5 m from the contact).

3. GEOCHRONOLOGY

A thin section of the dolerite dyke was observed prior to the geochronological experiments (Fig. 3). The groundmass (ca. 0.05–0.1 mm in diameter) comprised plagioclase, clinopyroxene, and opaque minerals with plagioclase and clinopyroxene phenocrysts (<1.8 mm) with nearly the same abundances. The remains of a porphyritic structure of igneous origin were evident, and no traces of regional metamorphism, such as changing mineral assemblage and/or systematic deformation, were observed. The trend of the long axis of each mineral was almost random. Although the alteration was minor, small amounts of actinolite, biotite, and limonite were found as alteration minerals. Actinolite replaced some of the outermost thin rims of the clinopyroxene phenocrysts and clinopyroxene in the groundmass. Small actinolite aggregates sometimes filled the small irregular cracks. Biotite was found close to opaque minerals in the groundmass. Limonites filled the minor and irregular cracks in the phenocrysts and groundmass, especially near opaque minerals.

We carried out $^{40}Ar/^{39}Ar$ dating of the individual clinopyroxene grains in the dolerite sample. The step-heating method of $^{40}Ar/^{39}Ar$ dating was applied to five clinopyroxene crystals approximately 0.5 mm in size. The details of the dating are described in the Appendix.

Four grains showed plateau ages between 1,808 and 1,887 Ga (Table 1, Fig. 4) for over 61–78% of the total argon released. The results from GP70-1 were eliminated for further analyses because the temperature control for step heating was unsuccessful. The total ages of each sample were calculated using the total gas fraction during the plateau age. The age of GP70-02 was slightly different from that of the others, possibly due to excess argon. The calculated mean of consistent three ages without this outlier was 1,816.0 ± 14.6 Ma (2σ). The dyke was thus intruded after the end of the Nagssugtoqidian orogeny.

4. ROCK MAGNETIC EXPERIMENTS

Stepwise isothermal remanent Magnetization (IRM) acquisition and thermal demagnetization of the composite IRMs acquired along three perpendicular axes (Lowrie, 1990) were performed on two dyke samples from sites GP72 and GP75. The presence of low-coercivity magnetic minerals with an unblocking temperature of approximately 580°C was prominent during these experiments (Fig. 5), indicating titanium-poor magnetite as a dominant magnetic mineral.

Seven samples from the eastern margin (site GP72) were subjected to thermomagnetic analyses (Js-T) in air using a Curie balance. The Js-T curves also revealed Curie temperatures of approximately 580°C. Few mineral changes occurred, although the experiments were performed in air.

To confirm the presence of titanium-poor magnetite, thin sections were observed under a JEOL JSM-7600F scanning electron microscope (SEM). Fe–Ti oxide grains exhibited low- to moderate-grade high-temperature oxidation, leading to the formation of titanium-poor magnetite subdivided by exsolution lamellae of ilmenite with widths of ~1 μm or higher (Fig. 6). According to Haggerty (1991), both trellis- and sandwich-type intergrowths of ilmenite were observed, and the oxidation states of the grains generally ranged from C2 (magnetite subdivided by a small number of exsolution lamellae of ilmenite) to C4 (magnetite subdivided by exsolution lamellae of ilmenite with incipient alteration to titanohematite). These features formed as a result of high-temperature deuteric oxidation. Additional energy dispersive X-ray (EDX) analyses confirm this interpretation qualitatively on the basis of the Fe/Ti ratios of the two different phases.

Hysteresis parameters were determined for the dyke samples using a vibrating sample magnetometer at Kyoto University in order to examine the domain state (Fig. 7). Measurements were applied to one specimen from each block sample from site GP72 and a representative specimen from site GP75. Data from almost all the specimens were distributed in a small cluster in pseudo-single domain (PSD) area on the Day plot

(Day et al., 1977), although the plot does not necessarily indicate the domain size (e.g. Dunlop, 2002). The bulk domain state (BDS) values (Paterson et al., 2017) for these samples were calculated to be between 0.25 and 0.35, and reliable Thellier paleointensity measurements were expected. An outlier on the plot may have been due to alteration of the sample, judging from the rather small Ms and Mr values. Other specimens from this block sample were eliminated from further work.

5. PALEOMAGNETIC DIRECTION

Natural remanent magnetization (NRM) of the samples was measured by a spinner magnetometer or a SQUID magnetometer depending on their intensity. More than ten specimens from both dyke and host rocks were demagnetized thermally in 15 heating steps up to 600°C (Fig. 8). Susceptibility was also measured after each step of the thermal demagnetization. At least one specimen from each site was demagnetized in alternating fields (AF). The results were analyzed using principal component analysis (Kirschvink, 1980) without anchoring to the origin.

Specimens from the eastern margin (GP72) had a well-defined high-temperature component (Fig. 8-a, Table 2). A low-temperature component with a roughly northerly direction with steep downward inclination was eliminated up to 300°C. The characteristic high-temperature component was isolated above 350–400°C and unblocked at 580°C. This characteristic direction was also observed during AF demagnetization above 35 mT. The mean direction of the characteristic high-temperature component from nine specimens was D = 242.4° and I = 67.4°, with the radius of the 95% confidence circle (α_{95}) of 6.3°.

Specimens from the western margin of the dolerite dyke (GP75) had characteristics of lightning remagnetization. The intensity before demagnetization was at least an order of magnitude more intense than that of specimens from GP 72. The directions of the high-coercivity component above 15 mT agreed well with the characteristic high-temperature directions from site GP72 (Figs. 8-b–d, Fig. 9; Table 2). The high-coercivity direction seemed to be that of the characteristic original component before the lightning because the overprinting by lightning strike can be successfully demagnetized by the AF procedure (Dunlop and Özdemir, 1997). Thermal demagnetization is not effective for isolating the characteristic direction. The experiments yielded gently curved or straight demagnetization paths to the origin (Figs. 8-c–d). The directions of high-temperature components had large scatter and did not agree with those of the high-coercivity components (Fig. 9), although a few specimens had behavior similar to that of GP72 (Fig. 8-b).

The characteristic directions were obtained through thermal demagnetization from GP72 and through AF demagnetization from GP75. The mean direction of the 17 specimens was D = 243.6° and I = 66.3°, with α_{95} of 3.9°. The direction yielded a virtual geomagnetic pole (VGP) of 33.5°N and 96.4°W. Samples from GP75 were excluded from the paleointensity study.

From the host rocks (GP71, GP73, GP74), we had no stable magnetic component. The intensity before demagnetization was rather small (~5 × 10^{-8} Am^2). We therefore could not do the baked contact test in this study.

6. PALEOINTENSITY

A total of 28 specimens from site GP72 were subjected to Thellier–Thellier-type experiments. The experiments followed the IZZI protocol of Tauxe and Staudigel (2004) in order to detect the influence of the multidomain particles. Routine checks of the reproducibility of partial thermal remanence acquisition (pTRM checks) were applied every Zero field–In field (ZI) step with some tail-check steps (Riisager and Riisager, 2001) on several specimens. Heating was performed in air and the magnetic field of 15 μT was chosen. These experiments were performed at The Center for Advanced Marine Core Research, Kochi University.

Paleointensity data were analyzed using the Arai plot and Thellier Tool 4.0 computer program (Leonhardt et al., 2004). The following criteria were used to assess the quality of the experimental data:

(1) The temperature range of the linear fit had to match that of the characteristic component identified during thermal demagnetization experiments.

(2) The angular difference between anchored to the origin and non-anchored direction (α) should be less than 15°.

(3) The MAD value (Kirschvink, 1980) for selected data should be lower than 10°.

(4) A minimum of six data points should be fulfilled for a linear fit.

(5) A pTRM test [δ(CK)] should give a positive result for a linear segment within 5% of the total thermal remanent magnetization(TRM, original).

(6) At least 30% of the NRM (f-fraction) has to be covered by a linear fit.

(7) The change in magnetic susceptibility should be less than 20% of the original value for a temperature range of the linear segment on the Arai plots.

(8) The scatter statistics β: The standard error of the slope over the absolute value of the best fit slope should be less than 0.15.

Thirteen out of thirty-five specimens passed the abovementioned criteria (Table 3). The results of the paleointensity experiments for the representative specimens are depicted in Fig. 10. The mean paleointensity obtained from reliable specimens was 14.8 ± 2.3 μT (1σ Standard deviation), where the calculated values varied between 12.0 and 19.0 μT. The Qpi value (Biggin and Paterson, 2014; Kulakov et al., 2019) was estimated to be 6. The data passed the age, DIR, STAT, TRM, ALT, and MD criteria.

In some samples, the demagnetization paths did not exhibit the straight decay to the origin, although the difference angles (α) passed the criterion of 15°. This phenomenon may be attributed to some residual of the laboratory-induced TRM due to the presence of MD grains. However, the pTRM tail-check parameters (δt*; Leonhardt et al., 2004) were less than 4.1 in all 13 specimens that passed the criteria. The δt* values were reasonably small, indicating that the influence of MD grains was likely minor. There was no correlation between the intensity and the value of the difference angles (αs). The mean of the intensity of samples with difference angles (α) between 15 and 10° (14.5 μT) was not significantly different from the mean value of the remaining ($\alpha < 10°$) samples (15.4 μT).

MD particles generally showed zigzagging behavior on the Arai plots using the IZZI method. To test the effects of zigzag on intensity determination, we calculated the slope of the Arai plot using three methods: 1) taking all points for the least square fit calculation, 2) taking only the Zero field-In field (ZI) points, and 3) taking only the In field-Zero field (IZ) points. The mean intensity from the ZI point calculations was 14.8 ± 3.2 μT and that from the IZ points was 17.0 ± 3.5 μT. The difference in slope calculation using the three methods was insignificant, implying that the quality of the Arai plots for intensity calculation was not affected by the zigzags. The degree of zigzag was considerably small in the specimens that passed the criteria, whereas some specimens that did not pass the criteria showed fairly large zigzags.

The concave feature on the Arai plots (Fig.10) was likely due to the alteration of the rocks at higher temperatures. The higher-temperature steps were excluded in determining paleointensity values because the pTRM tests failed. The concave feature could be partly due to the existence of MD particles remaining after the demagnetization at higher temperatures (Biggin, 2006). The intensity value of 14.8 μT could indicate some overestimation because the intensity values were calculated from the lower-temperature side of the concave curve.

As reported by Biggin et al. (2007), variation in cooling rate might cause an underestimation of paleointensity in non-SD material. However, samples used for this study were collected from the margin of the dyke, which is spread over a limited zone several tens of meters wide. As a result, the effects of cooling-rate variation on our samples were likely negligible. Macouin et al. (2003) also found no cooling-rate influence on the acquisition of magnetization for a 250-m-wide dyke.

7. DISCUSSION

7.1 Paleomagnetic Direction

The characteristic mean direction (D = 243.6°, I = 66.3°) at 1,816 Ma was compared with the directions of previously studied ~2.8 Ga and 2.6 Ga dolerite dykes in the Nuuk area (Morimoto et al., 1997; Miki et al., 2009; Fig. 11, Table 4). The primary nature of the older dyke samples was ascertained by contact tests. Compared with the country rock, the directions of the three dykes were clearly different from that of the ~3 Ga Nuuk gneiss (Morimoto et al., 1997; Miki et al., 2009; Fahrig and Bridgewater, 1976). These facts imply that no regional remagnetization events occurred in the Nuuk area where these three dykes are distributed and that the paleomagnetic directions of these dykes were acquired primarily at the periods of intrusion.

It is interesting to note that the paleomagnetic directions of the three Proterozoic dolerite dykes from Nuuk were distributed in a limited range within 12°, although they had different age data (1,816 Ma, this study; 2,585 Ma, Miki et al., 2009; 2,800 Ma, Morimoto et al., 1997). Nilsson et al. (2019) reported a U-Pb baddeleyite age of 2,125 ± 9 Ma from the same sample of the 2,585 Ma dyke in Miki et al. (2009). Even if the U-Pb age is adopted, the age of 2,125 Ma falls between 2.8 Ga and 1.8 Ga as the age of 2,585 Ma. Similar geomagnetic field directions are preserved at a period between ~2.5 Ga and 1.8 Ga in the Nuuk area, although the data are spot readings because the geomagnetic secular variations were not averaged out for the three dykes.

Similar paleomagnetic directions have also been reported from dolerite dykes (Kangamiut dykes) in the Nagssugtoqidian fold belt, 200 km north of the present study area. Fig. 12 and Table 5 show the VGPs of the metamorphosed Kangamiut dykes from Nagssugtoqidian Orogen (1.7–1.8 Ga pole, which was calculated based on the paleomagnetic direction of Piper 1981, 1985; Morgan 1976; Beckman, 2013) and from unmetamorphosed Southern Nagssugtoqidian Front (SNF; 2.04 Ga pole; Fahrig and Bridgewater 1976), together with those from the dolerite dykes in the Nuuk area (this study, Morimoto et al., 1997, Miki et al., 2009). The 1.7–1.8 Ga age of the poles from the orogen is the hornblende Ar–Ar age (Willigers et al., 1999) which is recognized to be the cooling age down after the orogenic event (the temperatures reached approximately 500°C), whereas the 2.04 Ga from the unmetamorophosed dyke is recognized to be the age of intrusion of the dyke (Willigers et al, 1999). Thus, the Proterozoic poles from southwestern Greenland are close to each other both spatially and temporally. The poles seem to have stayed at similar positions between 2.5 Ga and 1.7 Ga.

A long-term immobility of Paleoproterozoic pole positions is observed from the Australian craton. Fig. 13 shows the Paleoproterozoic poles from the Pilbara Craton in Australia. The pole moves only 25° during the 868 Myrs between 2,718 Ma and 1,850 Ma, although the poles moved moderately between 2,860 Ma and 2,718 Ma (Schmidt and Embeleton, 1985; Schmidt and Clark, 1994; Strik et al., 2003; Williams et al., 2004). Because the immobility in paleomagnetic pole positions is observed at two cratons, this characteristic maybe a peculiar phenomenon in the specific period between 2.7 Ga and 1.7 Ga of the Paleoproterozoic era.

In contrast to the stagnation of the paleomagnetic pole movements of Greenland in the North Atlantic and Australian Cratons, the poles from the Superior and Slave Craton moved separately and dynamically more than 160° during the 600 Myrs between 2.47 Ga and 1.88 Ga (Buchan et al., 2009; Buchan, 2013, Buchan et al., 2016; Mitchell et al., 2014) (Fig. 12). This rate of movement is the same as that of the Eurasian continent during last 200 Myrs (Besse and Courtillot, 2002), indicating that plate tectonic processes were in operation (Mitchell et al., 2014; Buchan et al., 2016). The comparison of the poles suggests that the Superior and Slave Cratons had considerably different tectonic behaviors from those of the stagnant North Atlantic and Australian Cratons between 2.47 and 1.88 Ma in the Paleoproterozoic. We found that the swift motion and motionless features of the cratons on the globe coexist, which may represent a premature mechanism of plate tectonics in ancient times.

Comparing the APWPs for the North Atlantic, Superior, and Slave Cratons around 1.8–1.7 Ga, the poles gathered in the same region near the south of North America (Fig. 12). The cratons seem to have amalgamated by ~1.7 Ga. The age of 1.7 Ga agrees with the assembly of Nuna supercontinent, which existed at approximately 1.5 Ga (e.g. Hoffman, 1997). The bulk of Nuna, including the North China Craton, appears to have formed by 1.75 Ga (Zhang et al., 2012; Xu et al., 2014).

7.2 Paleointensity

The virtual dipole moment (VDM) calculated for 1.8 Ga Greenland from the mean paleointensity and mean inclination (66.3°) was $2.88 \pm 0.46 \times 10^{22}$ Am^2. This value is approximately one-third of the present-day Earth's field strength ($\sim 8 \times 10^{22}$ Am^2). The present paleomagnetic results provide additional evidence for the small VDM value at the period of about 1.8 Ga. The VDM value of this study (1.816 Ga) is almost the same as that of a 1.786 Ga gabbro from Central Sweden (2.56 ± 0.33 × 10^{22} Am^2; Donadini et al., 2011) and that of 1.9 Ga dykes from South Africa (2.82 × 10^{22} Am^2; Shcherbakova et al., 2014). Low values are also reported from 1,782–1,795 Ma mafic sills from Amazonian Craton (1.3–6 × $10^{22}$$Am^2$, Chiara et al., 2017). The similar VDM values from the different Cratons and different rock types indicate that the low paleointensity (2.5–2.9 × $10^{22}$$Am^2$) is ascribed to a weak geomagnetic dipole field at approximately 1.8 Ga.

The very long-term variation of the geomagnetic field between 3,500 Ma and 1,000 Ma is described as a “well-shaped,” as suggested by Biggin et al. (2009; 2015). Fig. 14 displays the paleointensity data in the Precambrian era from the PINT(Qpi) database (Biggin et al., 2009; Biggin and Peterson 2014; Veikkolainen et al., 2017) with the value in this study (a star in the figure). The data with Qpi >= 3 were chosen. A low period between 2,400 and 1,400 Ma (3.0 ± 0.8 × 10^{22} Am^2, Biggin et al., 2015) is sandwiched between periods of higher intensity (4.4 × 10^{22} Am^2 before 2,400 Ma and 5.4 × 10^{22} Am^2 after 1,300 Ma). The VDM value of 2.88 ± 0.46 × 10^{22} Am^2 in this study is almost equivalent to the low value, with an average of 3.0 × 10^{22} Am^2 at the bottom of the well between 2,400 and 1,400 Ma.

A decrease occurring approximately 2,500 Ma in the well-shaped variation may indicate calming of the geodynamo activity. One possible explanation for the weak geodynamo is the decrease in thermal convection in the liquid core (Labrosse and Macouin, 2003; Aubert et al., 2009; Labrosse, 2015; Olson et al., 2015). Labrosse (2015) predicted a gradual decrease of the dipole moment by secular cooling from 4.5 Ga until inner core nucleation. An alternative explanation is the decrease caused by a sudden increase in the thermal conductivity of the core, which would reduce the thermal convection in the core (Hirose et al., 2017) and cause the abrupt decrease of the geomagnetic field. The long, low geomagnetic field from 2,400 to 1,300 Ma possibly reflects weak geodynamo activity due to inactive or no convection of the liquid core. As suggested by Ziegler and Stegman (2013), the low geomagnetic field can be maintained from the basal magma ocean layer in the lowermost mantle instead of the liquid core. Rejuvenation of geodynamo activity in the later period of the well-shaped variation of 1,300 Ma may be indicative of the formation of a solid inner core (Nakagawa and Tackley, 2010; 2013; Labrosse, 2015; Olson et al., 2015, Biggin et al., 2015). However, Smirnov et al. (2016) doubt the 1,300 Ma increase in the geomagnetic field because of the possibility of overestimation due to the inclusion of unreliable paleointensity results. Recently, the higher paleointensity value from the 1,300 Ma Gardar basalts of Greenland (Thomas, 1993) has been revised to a somewhat lower value (Kodama et al., 2019). An extremely low VDM value (~0.7× 10^{22} Am^2) has been reported from ~565 Ma intrusive rocks (Bono et al., 2019). The duration of small geomagnetic field could continue to a younger age.

8. CONCLUSION

Reliable paleomagnetic and geochronological results were obtained from an Early Proterozoic dolerite dyke, which intruded into the Archean Gneiss of the Nuuk area, southern West Greenland. The conclusions are as follows:

(1) Clinopyroxene grains from the dyke yielded Ar–Ar plateau ages from 1,808 to 1,887 Ma, with a mean value of 1,816.0 ± 14.6 Ma (2σ), indicating the younger generation of the Proterozoic dyke in southern West Greenland.

(2) The stable primary components of paleomagnetic direction were obtained from the dolerite dyke. Early Proterozoic paleomagnetic poles from southern West Greenland indicated that the North Atlantic Craton of southern Greenland may have been in the same position between approximately 2,500 Ma and 1,700 Ma. The North Atlantic Craton was motionless, whereas the Slave and Superior Cratons moved a long distance prior to 1.7 Ga.

(3) Thellier experiments yielded a mean paleointensity value of 14.8 ± 2.3 μT, indicating a VDM value of 2.88 ± 0.46 × 10^{22} Am^2. This value is approximately one-third of the present-day Earth's field intensity. The low value characterized the global paleointensity at the period of about 1.8 Ga.

ACKNOWLEDGMENTS

The authors would like to thank Professor Naoto Ishikawa (Kyoto University) for providing his laboratory facilities. A part of this study was performed under the cooperative research program of the Center for Advanced Marine Core Research (CMCR), Kochi University (08B034).

REFERENCES

Aubert, J., Labrosse, S. & Poitou, C., 2009. Modelling the palaeo-evolution of the geodynamo, Geophys. J. Int., 179, 1414–1428.

Beckmann, G.E.J., 2013. New interpretations on palaeomagnetic data from the Nagssugtoqidian mobile belt in Greenland, Precambrian Res., 224, 304– 315.

Besse, J. & Courtillot, V., 2002. Apparent and true polar wander and the geometry of the geomagnetic field in the last 200 million years, J. geophys. Res., 107, 1–31.

Biggin, A.J., 2006. First-order symmetry of weak-field partial thermoremanence in multi-domain (MD) ferromagnetic grains: 2. Implications for Thellier-type palaeointensity determination, Earth Planet. Sci. Lett., 245, 454–470.

Biggin, A.J., Perrin M. & Dekkers, M.J., 2007. A reliable absolute palaeointensity determination obtained from a non-ideal recorder, Earth Planet. Sci. Lett., 257, 545–563.

Biggin, A.J., Strik, G.H.M.A. & Langereis, C.G., 2009. The intensity of geomagnetic field in the late-Archaean: new measurements and an analysis of the updated IAGA palaeointensity database, Earth Planets Space, 61, 9–22.

Biggin, A. J. & Paterson, G. A., 2014. A new set of qualitative reliability criteria to aid inferences on palaeomagnetic dipole moment variations through geological time, Frontiers Earth Sci., 2, 1–9. doi.org/10.3389/feart.2014.00024

Biggin, A. J., Piispa, E. J., Pesonen, L.J., Holme, R. Paterson, G.A Veikkolainen, T. & Tauxe, L.,2015. Palaeomagnetic field intensity variations suggest Mesoproterozoic inner-core nucleation, Nature 526, 245-248.

Bono, R. K., Tarduno, J. A., Nimmo, F. & Cottrell R. D. ,2019. Young inner core inferred from Ediacaran ultra-low geomagnetic field intensity, Nature Geoscience 12, 143–147.

Bridgewater, D., Keto, L., McGregor, V.R. & Myers J.S., 1976. Archaean Gneiss complex of Greenland, in Geology of Greenland, pp. 19–75, eds Escher, A. & Watt, W. S., Geological Survey of Greenland, Copenhagen.

Buchan, K. L., 2013. Key paleomagnetic poles and their use in Proterozoic continent and supercontinent reconstructions: A review, Precambrian Res., 238, 93–110.

Buchan, K.L., LeCheminant, A.N. & van Breemen, O., 2009. Paleomagnetism and U–Pb geochronology of the Lac de Gras diabase dyke swarm, Slave Province, Canada:

implications for relative drift of Slave and Superior provinces in the Paleoproterozoic, Can. J. Earth Sci. 46, 361–379.

Buchan,K.L., Mitchell,R. N. Bleeker,W., Hamilton, M.A.& LeCheminante,A.N., 2016. Paleomagnetism of ca. 2.13–2.11 Ga Indin and ca. 1.885 Ga Ghost dyke swarms of the Slave craton: Implications for the Slave craton APW path and relative drift of Slave, Superior and Siberian cratons in the Paleoproterozoic,.Precambrian Res. 275,151–175.

Chiara, A.Di., Muxworthy, A. R., Trindade, R. I. F. & Bispo-Santos, F., 2017. Paleoproterozoic Geomagnetic Field Strength from the Avanavero Mafic Sills, Amazonian Craton, Brazil, Geochem. Geophys. Geosyst., 18. https://doi.org/10.1002/2017GC007175

Coe, R. S., Gromme, S. & Mankinen, E. A., 1978. Geomagnetic Paleointensities from the Radiocarbon-Dated Lava Flows on Hawaii and the Question of the Pacific Non-Dipole Low, J. Geophys. Res., A83 (B4), 1740–1756.

Condie, K.C., 2018. A planet in transition: The onset of plate tectonics on Earth between 3 and 2 Ga?, Geoscience Frontiers, 9, 51-60.

Connelly, J.N., van Gool, J.A.M. & Mengel, F.C., 2000. Temporal evolution of a deeply eroded orogen: the Nagssugtoqidian Orogen, West Greenland, Can. J. Earth Sci., 37, 1121–1142.

Day, R., Fuller, M. & Schmidt, V.A., 1977. Hysteresis properties of titanomagnetites: grain size and composition dependence, Phys. Earth Planet. Inter., 13, 260–267.

Donadini, F., Elming, S.-A., Tauxe, L. & Halenius, U., 2011. Paleointensity determination on a 1.786 Ga old gabbro from Hoting, Central Sweden, Earth Planet. Sci. Lett., 309, 234–248.

Dunlop, D.J., 2002. Theory and application of the Day plot (Mrs/Ms versus Hcr/Hc) 1. Theoretical curves and tests using titanomagnetite data, J. Geophys. Res. 107, 2056, doi: 10.1029/2001JB000486.

Dunlop, D. J., & Özdemir, Ö., 1997. Rock Magnetism: Fundamentals and Frontiers, 573 pp., Cambridge Univ. Press, New York.

Fahrig, W.F. & Bridgewater, D., 1976. Late Archean-Early Proterozoic paleomagnetic pole positions from West Greenland, in The Early History of the Earth, ed.Windley, B. F., pp 427–439, JohnWiley and Sons, London.

Friend, C.R.L., Nutman, A.P., Baadsgaard, H., Kinny, P.D. & McGregor, V.R., 1996. Timing of late Archaean terrane assembly, crustal thickening, and granite emplacement in the Nuuk region, southern West Greenland, Earth Planet. Sci. Lett., 142, 353-365.

Friend, C.R.L. & Nutman, A.P., 2005. New pieces to the Archean terrane jigsaw puzzle in the Nuuk region, southern West Greenland: steps in transforming a simple insight into a complex regional tectonothermal model. J. Geol. Soc., 162, 147-162.

Haggerty, S.E., 1991. Oxide textures—a mini-atlas. In: Lindsley, D.H.(Ed), Oxide Minerals: Petrologic and Magnetic Significance. Reviews in Mineralogy 25, Mineralogical Society of America, pp. 129-219.

Hall, R.P. & Hughes, D.J., 1987. Noritic dykes of southern Greenland: early Proterozoic boninitic magmatism. Contrib. Mineral. Petrol. 97, 169–182.

Hall, R.P. & Hughes, D.J., 1990. Precambrian mafic dykes of southern Greenland. In: Parker, A.J., Rickwood, P.C., Tucker, D.H. (Eds.), Mafic Dykes and Emplacement Mechanism. A.A. Balkema, Rotterdam, pp. 481–495.

Hamilton W.B. 2011. Plate tectonics began in Neoproterozoic time, and plumes from deep mantle have never operated. Lithos 123, 1–20.

Hirose, K., Morard, G. Sinmyo, R., Umemoto, K., Hernlund, J., Helffrich, G. & Labrosse, S., 2017. Crystallization of silicon dioxide and compositional evolution of the Earth’s core, Nature 543, 99–102.

Hoffman, P.F., 1997. Tectonic genealogy of North America. In Earth structure. In: van der Pluijm, B.A., Marshak, S. (Eds.), An Introduction to Structural Geology and Tectonics. McGraw-Hill, New York, pp. 459‐464.

Hyodo, H., Matsuda, T., Fukui, S. & Itaya, T., 1994. 40Ar/39Ar age determination of a single mineral grain by Laser step heating, Bull. Res. Inst. Nat., Okayama Univ. of Sci., 20, 63–67.

Hyodo, H., Itaya, T. & Matsuda, T., 1995. Temperature measurement of small minerals and its precision using Laser heating, Bull. Res. Inst. Nat., Okayama Univ. Sci., 21, 3–6.

Hyodo, H., Kim, S., Itaya, T. & Matsuda, T., 1999. Homogeneity of neutron flux during irradiation for 40Ar/39Ar age dating in the research reactor at Kyoto University, J. Miner. Petrol. Econ. Geol., 94, 329–337.

Kalsbeek, F., & Nutman, A. 1996. Anatomy of the Early Proterozoic Nagssugtoqidian Orogen, West Greenland, explored by reconnaissance SHRIMP U-Pb zircon dating, Geology 24, 515–518.

Kalsbeek, F., Taylor, P.N., & Henriksen, N., 1984. Age of rocks, structures and metamorphism in the Nagssugtoqidian mobile belt, West Greenland—Field and Pb isotope evidence: Can. J. Earth Sci. 21, 1126–1131.

Kalsbeek, F., Pidgeon, R. T. & Taylor, P. N. 1987. Nagssugtoqidian mobile belt of West Greenland: a cryptic 1850 Ma suture between two Archaean continents—chemical and isotopic evidence. Earth Planet.Sci. Lett. 85, 365–385.

Kirschvink, J.L., 1980. The least-squares line and plane and the analysis of palaeomagnetic data, Geophys. J. R. astr. Soc., 62, 699–718.

Kodama, K. P., Carnes L. K., Tarduno, J. A., Berti, C., 2019. Palaeointensity of the 1.3 billion-yr-old Gardar basalts, southern Greenland revisited: no evidence for onset of inner core growth, Geophys. J. Int., 217, 1974-1987, doi: 10.1093/gji/ggz126.

Korenaga, J., 2013. Initiation and Evolution of Plate Tectonics on Earth: Theories and Observations, Annu. Rev. Earth Planet. Sci., 41, 117–151.

Kurakov, E. V., Sprain, C. J., Doubrovine, P. V., Smirnov, A. V., Paterson, G. A., Hawkins, L., Fairchild, L., Piispa, E. J., Biggin, A. J., 2019. Analysis of an Updated Paleointensity Database (QPI - PINT) for 65-200 Ma: Implications for the Long - Term History of Dipole Moment Through the Mesozoic, J. Geophys. Res: Solid Earth, 124, 9999-10022, doi.org/10.1029/2018JB017287.

Labrosse, S., 2015. Thermal evolution of the core with a high thermal conductivity, Phys. Earth Planet. Inter. 247 36–55.

Labrosse, S. & Macouin, M., 2003. The inner core and the geodynamo. C. R. Geosci. 335, 37–50.

Leonhardt, R., Heunemann, C. & Krasa, D., 2004. Analyzing absolute paleointensity determinations: acceptance criteria and the software ThellierTool4.0, Geochem. Geophys. Geosyst., 5, Q12016, doi:10.1029/2004GC000807.

Lowrie, W., 1990. Identification of ferromagnetic minerals in a rock by coercivity and unblocking temperature properties, Geophys. Res. Lett.,17, 159–162.

Macouin, M., Valet, J.P., Besse, J., Buchan, K., Ernst, R., LeGoff, M. & Scharer, U., 2003. Low paleointensities recorded in 1 to 2.4 Ga Proterozoic dykes, Superior Province, Canada. Earth planet. Sci. Lett., 213, 79–95.

Marker, M., Mengel, F.C., van Gool, J.A.M. & field party 1995. Evolution of the Palaeoproterozoic Nagssugtoqidian orogen: DLC investigations in West Greenland. Rapport Grønlands Geologiske Undersøgelse 165, 100‑105.

Miki, M., Taniguchi, A., Yokoyama, M., Gouzu, C., Hyodo, H., Uno, K., Zaman, H., Otofuji, Y., 2009. Palaeomagnetism and geochronology of the Proterozoic dolerite dyke from southwest Greenland; indication of low palaeointensity. Geophys. J. Int. 179, 18–34.

Mitchell, R.N., Bleeker, W., van Breemen, O. V., Lecheminant, T. N., Peng, P.E, Nilsson, M.K.M & Evans,D.A.D., 2014. Plate tectonics before 2.0 Ga: Evidence from paleomagnetism of cratons within supercontinent Nuna, American J. Sci., 314, 878–894.

Morgan, G.E., 1976. Palaeomagnetism of a slowly cooled plutonic terrain in western Greenland. Nature 259, 382–385.

Morimoto, C., Otofuji, Y., Miki, M., Tanaka, H. & Itaya, T., 1997. Preliminary palaeomagnetic results of an Archaean dolerite dyke of west Greenland: geomagnetic field intensity at 2.8 Ga, Geophys. J. Int., 128, 585–593.

Nakagawa, T. & Tackley, P. J., 2010. Influence of initial CMB temperature and other parameters on the thermal evolution of Earth's core resulting from thermochemical spherical mantle convection, *Geochem. Geophys. Geosyst.*, **11**, Q06001, doi:10.1029/2010GC003031.

Nakagawa, T. & Tackley, P. J.,2013. Implications of high core thermal conductivity on Earth's coupled mantle and core evolution, *Geophys. Res. Lett.*, **40**, 2652–2656.

Nier, A.O., 1950. A redetermination of the relative abundances of the isotopes of carbon, nitrogen, oxygen, argon, and potassium. Physical Reviews 77, 789–793.

Nilsson, M.K.M., Söderlund, U., Ernst, R.E., Scherstén, A., Hamilton, M.A., Scherstén, A. & Armitage, P.E.B., 2010. Precise U–Pb baddeleyite ages of mafic dykes and intrusions in southern West Greenland and implications for a possible reconstruction with the Superior craton. Precambrian Res. 183, 399–415.

Nilsson, M.K.M., Klausen, M.B., Söderlund, U. & Ernst, R.E., 2013. Precise U–Pb ages and geochemistry of Palaeoproterozoic mafic dykes from southern west Greenland, Lithos 174,255–270.

Nilsson, M.K.M., Klausen, M.B. & Petersson, A., 2019. Break-up related 2170–2120 Ma mafic dykes across the North Atlantic craton: Final dismembering of a North Atlantic-Dharwar craton connection?, Precambrian Res., 329, 70-87.

Olson, P., Deguen, R., Rudolph, M. L. & Zhong, S., 2015. Core evolution driven by mantle global circulation, Phys. Earth Planet. Inter., 243, 44–55.

O'Neil, C., Lenardic A., Weller, M., Moresi, L., Quenette, S., & Zhang, S., 2016. A window for plate tectonics in terrestrial planet evolution?, Phys. Earth Planet. Inter., 255, 80-92,

Paterson G.A., Muxworthy A.R., Yamamoto Y. & Pan Y., 2017. Bulk magnetic domains stability controls paleointensity fidelity, Proc. Natl. Acad. Sci. USA , 114(50), 13 120–13 125. https://doi.org/10.1073/pnas.1714047114

Piper, J.D.A., 1981. The altitude dependence of magnetic remanence in the slowly-cooled Precambrian plutonic terrain of West Greenland, Earth Planet. Sci. Lett. 54, 449–466.

Piper, J.D.A., 1985. Palaeomagnetic study of the Nagssugtoqidian mobile belt in central-west Greenland, Precambrian Res., 28, 75-110.

Polat, A., Appel, P.W.U., Fryer, B.J., 2011. An overview of the geochemistry of Eoarchean to Mesoarchean ultramafic to mafic volcanic rocks, SW Greenland: Implications for mantle depletion and petrogenetic processes at subduction zones in the early Earth, Gondwana Res., 20, 255–283.

Riisager P., Riisager J., 2001. Detecting multidomain magnetic grains in Thellier palaeointensity experiments, Phys. Earth Planet. Inter., 125, 111–117.

Roddick, J.C., 1983. High precision intercalibration of ^{40}Ar-^{39}Ar standards, Geochim. Cosmochim. Acta, 47, 887–898.

Roest, W.R. & Srivastava, S.P., 1989. Sea-floor spreading in the Labrador Sea: A new reconstraction, Geology, 17, 1000-1003.

Schmidt, P.W. & Clark, D.A., 1994. Palaeomagnetism and magnetic anisotropy of Proterozoic banded-iron formations and iron ores of the Hamersley Basin, Western Australia, Precambrian Res., 69, 133‑155.

Schmidt, P.W. & Embleton, J.J., 1985. Prefolding and overprint magnetic signatures in Precambrian (~2.9‑2.7 Ga) igneous rocks from the Pilbara Craton and Hamersley Basin, NW Australia, J. Geophys. Res. 90, 2967‑2984.

Shcherbakova, V. V., Shcherbakov, V. P., Zhidkov, G. V., & Lubnina, N. V., 2014. Paleointensity determinations on rocks from Palaeoproterozoic dykes from the Kaapvaal Craton (South Africa). Geophys. J. Int., 197, 1371–1381.

Smirnov, A.V. Tarduno, J.A., Kulakov, E.V., McEnroe, S.A. & Bono, R.K., 2016. Paleointensity, core thermal conductivity and the unknown age of the inner core, Geophys. J. Int., 205, 1190-1195.

Steiger, R.H. & Jager, E., 1977. Subcommission on geochronology: convention on the use of decay constants in geo- and cosmochronology. Earth Planet. Science Letters 36, 359‑362.

Stern, R.J., 2008. Modern-style plate tectonics began in Neoproterozoic time: An alternative interpretation of Earth's tectonic history, in Condie, K.C., & Pease, V. eds., When Did Plate Tectonics Begin on Planet Earth?: Geological Society of America Spec. Pap., 440, p. 265–280.

Strik, G., Blake, T.S., Zegers, T.E., White, S.H. & Langereis, C.G., 2003. Palaeomagnetism of flood basalts in the Pilbara Craton, Western Australia: Late Archaean continental drift and the oldest known reversal of the geomagnetic field, J. Geophys. Res. 108, 2551, doi:10.1029/2003JB002475.

Taylor, P. N. & Kalsbeek, F., 1990. Dating the metamorphism of Precambrian marbles: Examples from Proterozoic mobile belts in Greenland, Chemical Geology (Isotope Geoscience Section), 86, 21–28.

Tauxe, L. & Staudigel, H., 2004. Strength of the geomagnetic field in the Cretaceous Normal Superchron: new data from submarine basaltic glass of the Troodos Ophiolite, Geochem. Geophys. Geosyst., 5, Q02H06, doi:10.1029/2003GC000635.

Thomas N., 1993. An integrated rock magnetic approach to the selection or rejection of ancient basalt samples for palaeointensity experiments, Phys. Earth planet. Inter., 75, 329–342.10.1016/0031-9201(93)90008-W

Veikkolainen, T. H., Biggin, A. J., Pesonen, L. J., Evans, D. A. & Jarboe, N. A., 2017. Data Descriptor: Advancing Precambrian palaeomagnetism with the PALEOMAGIA and PINT(QPI) databases, Sci. Data 4:170068 doi: 10.1038/sdata.2017.68.

Walker, F.W. Parrington, J.R. & Feiner, F., 1989. Nuclides and Isotopes, 14th ed. GE Nuclear Energy 57pp.

Williams, W.G., Schmidt, P.W. & Clark, D.A., 2004. Palaeomagnetism of iron-formation from the late Palaeoproterozoic Frere Formation, Earaheedy Basin, Western Australia: palaeogeographic and tectonic implications, Precambrian Res. 128, 367–383.

Willigers, B.J.A., Mengel, F.C., Bridgwater, D.,Wijbrans, J.R. & van Gool, J.A.M., 1999. Mafic dike swarms as absolute time markers in high-grade terranes: $^{40}Ar/^{39}Ar$ geochronological constraints on the Kangâmiut dikes, West Greenland. Geology 27, 775–778.

Willigers, B.J.A., Krogstad, E.J. & Wijbrans, J.R., 2001. Comparison of thermochronometers in a slowly cooled Granulite Terrain: Nagssugtoqidian Orogen, West Greenland, J. Petrol., 42, 1729–1749.

Willigers, B.J.A., van Gool, J.A.M., Wijbrans, J.R., Krogstad, E.J. & Mezger, K., 2002. Posttectonic Cooling of the Nagssugtoqidian Orogen and a Comparison of Contrasting Cooling Histories in Precambrian and Phanerozoic Orogens. J. Geol., 110, 503-517.

Windley, B. & Garde, A.A., 2009. Arc-generated blocks with sections in the North Atlantic craton of West Greenland: crustal growth in the Archean with modern analogues., Earth-Sci. Rev. 93, 1‐30.

Xu, H., Yang, Z., Peng, P., Meert, J.G. & Zhu, R. 2014. Paleo-position of the North China craton within the supercontinent Columbia: Constraints from new paleomagnetic results. Precambrian Res., 255, 276–293.

Zhang, S.-H., Li, Z.-X., Evans, D.A.D., Wu, H.-C., Li, H.-Y. & Dong, J., 2012. Pre-Rodinia supercontinent Nuna shaping up: A global synthesis with new paleomagnetic results from North China. Earth Planet. Sci. Lett. 353-354, 145–155.

Ziegler, L.B. & Stegman, D.R., 2013. Implications of a long-lived basal magma ocean in generating Earth’s ancient magnetic field, Geochem. Geophys. Geosyst., 14, 4735–4742.

APPENDIX: $^{40}Ar/^{39}Ar$ DATING OF CLINOPYROXENE GRAINS

Each crystal was placed in a 2-mm hole drilled on an aluminum tray together with a standard age sample (3 gr hornblende; Roddick 1983). Calcium ($CaSi_2$) and potassium salts (synthetic $KAlSi_3O_8$ glass) were also placed on the tray for Ca and K corrections. Subsequently, the tray was vacuum-sealed in a quartz tube. Samples were then exposed to neutron radiation for 8 h in the core of the 3 MW Research Reactor of Kyoto University (KUR) using the hydraulic rabbit facility (sample capsule transferring system with hydraulic pressure). The fastest neutron flux density was 3.9×10^{13} n/cm^2/s, which was confirmed to have remained uniform in the dimension of the sample holder (diameter 16 mm × height 15 mm) as little variation in the *J*-value of evenly spaced age standards was observed using the method of Hyodo et al. (1999). The average *J*-value and correction factors for potassium and calcium were $J = 0.00081930 \pm 0.00000615$ $(^{40}Ar/^{39}Ar)$ K = 0.3478 ± 0.0254, $(^{36}Ar/^{37}Ar)$ Ca = 0.00031854 ± 0.00011261, and $(^{39}Ar/^{37}Ar)$ Ca = 0.0010984 ± 0.0002614, respectively.

Each crystal was analyzed by the stepwise-heating technique using a 5-W continuous argon ion laser. Following this procedure, crystals were heated under a defocused laser beam at a given temperature for 30 s. The sample temperature was monitored by an infrared thermometer, which had a precision of 3°C within an area of 0.3 mm diameter

(Hyodo et al. 1995). The extracted gas was purified with a SAES Zr-Al getter (St 101), which was kept at 400°C for 5 min. Argon isotopes were then measured using a custom-made high-resolution mass spectrometer ([M/ΔM] > 400) that allows separation of the hydrocarbon peaks with the exception of mass 36 (Hyodo et al., 1994). Typical blanks of extraction lines for ^{36}Ar, ^{37}Ar, ^{38}Ar, ^{39}Ar, and ^{40}Ar were 5×10^{-14}, 3×10^{-14}, 3×10^{-14}, 3×10^{-14}, and 2×10^{-12} ccSTP, respectively.

Table 1 Ar/Ar data and constants in age calculations.

Sample: GP70-CPX1 Lab #: 100302A3 J : 8.193E-04 ± 6.15E-06 D : 1.005 Heating 60 s Sensitivity = 0.980 A/ccSTP
cpx

Temp.	CUM.39Ar	^{40}Ar (ccSTP)	σ40 (ccSTP)	^{39}Ar (ccSTP)	σ39 (ccSTP)	^{38}Ar (ccSTP)	σ38 (ccSTP)	^{37}Ar^{*2} (ccSTP)	σ37 (ccSTP)	^{36}Ar (ccSTP)	σ36 (ccSTP)	%^{40}Ar*	^{40}Ar*/^{39}Ar	σ4039	Age (Ma)	σ	^{37}Ar/^{39}Ar	σ3739	days
570	0.013	2.158E-10	4.454E-12	1.159E-13	3.029E-14	1.660E-13	3.289E-14	3.167E-11	3.623E-11	5.657E-14	2.732E-14	9.363E+01	2.491E+03	1.559E+03	2006.2	758.0	390.365	655.676	398
957	0.891	1.883E-08	3.446E-10	7.911E-12	1.390E-13	6.562E-12	1.471E-13	0.000E+00	4.956E-11	3.504E-13	5.784E-14	9.945E+01	2.367E+03	3.072E+01	1944.9	17.8	0	0	398
1478(fused)	1	5.356E-09	8.807E-11	9.815E-13	3.588E-14	5.263E-13	2.819E-14	-6.054E-11	3.284E-11	2.158E-13	3.917E-14	9.881E+01	5.391E+03	1.817E+02	3048.1	50.8	0	0	398
TOTAL		2.440E-08	4.208E-10	9.008E-12	1.612E-13	7.254E-12	1.622E-13	3.167E-11	6.961E-11	6.227E-13	7.571E-14	9.926E+01	2.699E+03	3.972E+01	2104.6	20.5	3.529	7.788	
Typical BLANK		3.138E-12	1.235E-12	1.504E-13	6.243E-15	2.336E-13	1.866E-14	1.699E-13	1.179E-14	4.733E-13	1.847E-14								

Sample: GP70-CPX2 Lab #: 100302A4 J : 8.193E-04 ± 6.15E-06 D : 1.005 Heating 60 s Sensitivity = 0.980 A/ccSTP
cpx

Temp.	CUM.39Ar	^{40}Ar (ccSTP)	σ40 (ccSTP)	^{39}Ar (ccSTP)	σ39 (ccSTP)	^{38}Ar (ccSTP)	σ38 (ccSTP)	^{37}Ar^{*2} (ccSTP)	σ37 (ccSTP)	^{36}Ar (ccSTP)	σ36 (ccSTP)	%^{40}Ar*	^{40}Ar*/^{39}Ar	σ4039	Age	σ	37/39	σ3739	
594	0.012	3.301E-10	5.477E-12	1.176E-13	3.505E-14	2.062E-13	2.840E-14	3.103E-11	4.061E-11	5.827E-14	3.934E-14	9.567E+01	3.781E+03	2.597E+03	2544.6	936.8	3.715E+02	7.031E+02	399
717	0.043	7.527E-10	1.208E-11	2.894E-13	4.294E-14	2.049E-13	3.253E-14	1.592E-11	5.806E-11	3.657E-14	3.224E-14	9.876E+01	2.733E+03	7.734E+02	2120.4	353.0	5.855E+01	2.274E+02	399
814	0.135	1.796E-09	2.816E-11	8.694E-13	3.975E-14	3.757E-13	3.987E-14	1.915E-10	7.077E-11	2.049E-14	3.314E-14	1.007E+02	2.725E+03	4.124E+02	2116.8	188.8	2.905E+02	1.442E+02	399
907	0.346	4.458E-09	7.019E-11	1.991E-12	5.355E-14	1.166E-12	3.561E-14	1.492E-11	4.520E-11	3.636E-14	4.764E-14	9.979E+01	2.252E+03	7.634E+01	1886.5	40.6	7.557E+00	2.308E+01	399
952	0.539	4.111E-09	6.878E-11	1.823E-12	4.014E-14	1.311E-12	4.422E-14	8.634E-12	4.598E-11	8.052E-14	4.340E-14	9.944E+01	2.254E+03	7.401E+01	1887.3	39.4	4.761E+00	2.549E+01	399
1030	0.655	2.481E-09	4.169E-11	1.100E-12	4.613E-14	7.204E-13	3.588E-14	-5.231E-11	6.280E-11	5.646E-14	3.649E-14	9.933E+01	2.240E+03	8.914E+01	1880.0	47.3	0.000E+00	0.000E+00	399
1088	0.779	2.612E-09	4.178E-11	1.163E-12	3.665E-14	7.867E-13	4.235E-14	-2.893E-11	5.354E-11	-7.825E-14	3.457E-14	1.000E+02	2.245E+03	6.237E+01	1882.6	33.6	0.000E+00	0.000E+00	399
573^{*3}	0.823	9.283E-10	1.660E-11	4.186E-13	2.626E-14	3.073E-13	2.778E-14	1.830E-11	4.515E-11	7.391E-15	3.500E-14	9.995E+01	2.328E+03	3.285E+02	1925.4	167.3	4.592E+01	1.190E+02	399
584^{*3}	1.000	8.946E-09	1.678E-10	1.673E-12	4.604E-14	1.197E-12	4.530E-14	2.414E-11	3.736E-11	3.764E-13	5.303E-14	9.878E+01	5.368E+03	1.928E+02	3041.6	54.0	1.466E+01	2.306E+01	399
TOTAL		2.642E-08	4.205E-10	9.445E-12	1.860E-13	6.276E-12	1.506E-13	3.044E-10	1.564E-10	6.724E-13	1.206E-13	9.936E+01	2.880E+03	7.109E+01	2186.4	32.7	3.342E+01	1.779E+01	
Typical BLANK		3.851E-12	4.832E-13	2.010E-13	2.794E-14	2.621E-13	2.590E-14	1.755E-13	1.187E-14	5.302E-13	2.969E-14								
Plateau Age (907°C−573°C, 68.8% of ^{39}Ar released):															1887	29			

Sample: GP70-CPX3 Lab #: 100302A5 J : 8.193E-04 ± 6.15E-06 D : 1.005 Heating 60 s Sensitivity = 0.980 A/ccSTP
cpx

Temp.	CUM.39Ar	^{40}Ar (ccSTP)	σ40 (ccSTP)	^{39}Ar (ccSTP)	σ39 (ccSTP)	^{38}Ar (ccSTP)	σ38 (ccSTP)	^{37}Ar^{*2} (ccSTP)	σ37 (ccSTP)	^{36}Ar (ccSTP)	σ36 (ccSTP)	%^{40}Ar*	^{40}Ar*/^{39}Ar	σ4039	Age (Ma)	σ	37/39	σ3739	days
597	0.027	1.071E-10	2.629E-12	7.902E-14	3.810E-14	1.084E-13	2.100E-14	5.732E-11	4.593E-11	3.396E-14	2.827E-14	9.567E+01	6.379E+03	2.580E+04	3299.4	6125.1	3.569E+03	1.675E+04	399
712	0.089	2.629E-10	4.477E-12	1.828E-13	2.907E-14	1.269E-13	2.908E-14	1.010E-10	6.299E-11	3.452E-14	3.042E-14	9.974E+01	3.650E+03	4.041E+03	2496.5	1497.0	1.406E+03	2.359E+03	399
810	0.239	9.062E-10	2.140E-11	4.434E-13	3.667E-14	1.894E-13	2.525E-14	6.969E-11	4.596E-11	2.008E-14	3.076E-14	1.001E+02	2.470E+03	4.374E+02	1996.1	214.0	1.900E+02	1.528E+02	399
904	0.6	2.355E-09	6.947E-11	1.065E-12	4.639E-14	5.956E-13	3.091E-14	-6.877E-11	3.034E-11	2.906E-14	2.976E-14	9.964E+01	2.203E+03	1.058E+02	1860.5	56.5	0.000E+00	0.000E+00	399
955	0.731	7.804E-10	1.226E-11	3.873E-13	4.928E-14	1.722E-13	2.051E-14	-6.793E-11	3.984E-11	6.967E-14	3.114E-14	9.736E+01	1.962E+03	2.490E+02	1728.8	141.4	0.000E+00	0.000E+00	399
1015	0.871	8.359E-10	1.328E-11	4.120E-13	4.384E-14	2.276E-13	2.020E-14	-1.297E-11	5.768E-11	6.229E-14	2.933E-14	9.780E+01	1.984E+03	2.100E+02	1741.3	118.5	0.000E+00	0.000E+00	399
1019	0.924	4.914E-10	8.573E-12	1.554E-13	3.211E-14	1.105E-13	3.551E-14	-1.609E-11	4.436E-11	8.022E-15	3.221E-14	9.952E+01	3.146E+03	6.516E+02	2299.7	269.4	0.000E+00	0.000E+00	399
1153	1	9.960E-10	1.984E-11	2.253E-13	2.970E-14	2.123E-13	3.925E-14	-1.622E-11	5.794E-11	8.794E-14	3.664E-14	9.739E+01	4.305E+03	5.684E+02	2724.3	185.9	0.000E+00	0.000E+00	399
TOTAL		6.735E-09	1.216E-10	2.951E-12	1.176E-13	1.743E-12	8.521E-14	2.280E-10	1.391E-10	3.456E-13	8.840E-14	9.880E+01	2.464E+03	1.812E+02	1993.4	89.17	84.448	56.422	
Typical BLANK		3.204E-12	1.396E-12	1.835E-13	2.702E-14	2.638E-13	1.345E-14	1.679E-13	1.575E-14	4.936E-13	2.393E-14								
Plateau Age (810°C−1015°C, 78.2 % of ^{39}Ar released):															1840	70			

Table 1 Continued

Sample: GP70-CPX4 Lab #: 100302A7 J : 8.193E-04 ± 6.15E-06 D : 1.005 Heating 60 s Sensitivity = 0.980 A/ccSTP
cpx

Temp.	CUM.39Ar	^{40}Ar (ccSTP)	σ40 (ccSTP)	^{39}Ar (ccSTP)	σ39 (ccSTP)	^{38}Ar (ccSTP)	σ38 (ccSTP)	^{37}Ar*2 (ccSTP)	σ37 (ccSTP)	^{36}Ar (ccSTP)	σ36 (ccSTP)	%^{40}Ar*	^{40}Ar*/^{39}Ar	σ4039	Age (Ma)	σ	37/39	σ3739	days
596	1.700E-02	1.073E-09	2.716E-11	4.409E-13	3.436E-14	3.360E-13	2.611E-14	4.726E-11	4.876E-11	6.788E-14	2.256E-14	98.55	2.718E+03	4.542E+02	2113.7	208.23	121.509	142.498	400
706	6.100E-02	2.996E-09	6.243E-11	1.119E-12	3.532E-14	5.817E-13	2.735E-14	0.000E+00	4.043E-11	2.120E-13	2.409E-14	97.91	2.623E+03	8.163E+01	2069.2	39.42	0	0	400
805	1.940E-01	6.527E-09	2.403E-10	3.390E-12	1.355E-13	1.163E-12	3.139E-14	1.832E-11	4.607E-11	1.424E-13	3.512E-14	99.38	1.925E+03	1.007E+02	1707.7	58.36	5.438	13.755	400
897	4.050E-01	1.116E-08	1.845E-10	5.385E-12	1.056E-13	2.871E-12	5.848E-14	5.160E-11	4.837E-11	3.172E-14	5.585E-14	99.96	2.093E+03	3.578E+01	1801.6	21.27	9.684	9.175	400
947	6.260E-01	1.158E-08	1.807E-10	5.627E-12	1.507E-13	5.301E-12	1.301E-13	3.854E-11	4.262E-11	8.606E-14	3.885E-14	99.81	2.068E+03	4.919E+01	1788.3	28.29	6.9	7.689	400
1004	8.060E-01	9.855E-09	1.680E-10	4.606E-12	9.280E-14	3.178E-12	9.816E-14	5.420E-11	5.835E-11	1.185E-13	3.614E-14	99.7	2.161E+03	4.502E+01	1838.4	25.53	11.923	13.003	400
1048	8.680E-01	3.612E-09	6.480E-11	1.574E-12	5.113E-14	9.484E-13	3.476E-14	2.759E-11	5.464E-11	1.406E-13	5.074E-14	98.92	2.314E+03	1.154E+02	1918.3	59.55	17.871	36.093	400
852*3	9.140E-01	2.967E-09	6.375E-11	1.167E-12	4.157E-14	1.355E-12	5.788E-14	-5.584E-11	4.271E-11	1.431E-13	3.999E-14	98.57	2.505E+03	8.950E+01	2013.3	44.28	0	0	400
1114	9.370E-01	2.154E-09	5.649E-11	5.979E-13	4.419E-14	5.006E-13	2.225E-14	-4.319E-11	4.316E-11	-5.630E-14	4.485E-14	100	3.602E+03	2.713E+02	2478.7	102	0	0	400
1300	1.000E+00	1.316E-08	8.395E-10	1.601E-12	6.996E-14	1.098E-12	6.007E-14	-1.262E-11	3.733E-11	4.513E-13	1.093E-13	98.99	8.137E+03	6.080E+02	3674.6	117.81	0	0	400
TOTAL		6.508E-08	1.319E-09	2.551E-11	4.625E-13	1.733E-11	3.406E-13	2.375E-10	1.476E-10	1.394E-12	1.649E-13	99.4	2.562E+03	4.541E+01	2040.6	23.52	9.408	5.904	
Typical BLANK		1.283E-12	8.606E-13	1.838E-13	1.985E-14	2.349E-13	1.553E-14	1.634E-13	1.106E-14	3.903E-13	1.590E-14								
Plateau Age (897°C−1004°C, 61.2% of ^{39}Ar released):															1808	17			

Sample: GP70-CPX5 Lab #: 100302A6 J : 8.193E-04 ± 6.15E-06 D : 1.005 Heating 60 s Sensitivity = 0.980 A/ccSTP
cpx

Temp.	CUM.39Ar	^{40}Ar (ccSTP)	σ40 (ccSTP)	^{39}Ar (ccSTP)	σ39 (ccSTP)	^{38}Ar (ccSTP)	σ38 (ccSTP)	^{37}Ar*2 (ccSTP)	σ37 (ccSTP)	^{36}Ar (ccSTP)	σ36 (ccSTP)	%^{40}Ar*	^{40}Ar*/^{39}Ar	σ4039	Age (Ma)	σ	37/39	σ3739	days
595	0.016	3.607E-10	6.442E-12	1.683E-13	3.123E-14	2.124E-13	2.377E-14	1.946E-11	5.726E-11	3.313E-14	3.456E-14	97.79	2.400E+03	1.151E+03	1961.4	573.8	132.432	447.21	401
716	0.055	1.018E-09	2.309E-11	4.086E-13	4.498E-14	2.766E-13	3.626E-14	2.267E-11	4.547E-11	6.982E-14	2.932E-14	98.18	2.605E+03	4.587E+02	2060.9	216.5	59.077	126.368	401
806	0.143	1.933E-09	4.260E-11	9.100E-13	4.150E-14	3.558E-13	2.027E-14	3.850E-11	4.748E-11	4.021E-14	3.677E-14	99.57	2.217E+03	1.725E+02	1868.1	91.0	44.372	57.419	401
902	0.349	4.592E-09	1.364E-10	2.149E-12	5.647E-14	1.000E-12	4.481E-14	5.884E-11	4.866E-11	6.774E-14	4.230E-14	99.68	2.195E+03	9.437E+01	1856.6	50.6	28.223	24.069	401
956	0.547	4.424E-09	1.094E-10	2.060E-12	6.946E-14	1.258E-12	4.205E-14	9.292E-12	4.851E-11	1.046E-13	4.530E-14	99.32	2.144E+03	9.520E+01	1829.1	51.8	4.534	23.786	401
1038	0.682	2.936E-09	5.076E-11	1.407E-12	4.758E-14	8.051E-13	4.503E-14	1.644E-11	4.647E-11	8.471E-14	4.111E-14	99.2	2.097E+03	1.021E+02	1803.9	56.2	11.837	33.902	401
1060	0.788	2.653E-09	6.219E-11	1.106E-12	4.706E-14	5.829E-13	3.006E-14	-1.316E-10	4.869E-11	-8.621E-14	3.636E-14	100	2.398E+03	1.041E+02	1960.6	52.7	0	0	401
1024	0.847	1.611E-09	3.328E-11	6.200E-13	3.968E-14	4.361E-13	3.223E-14	-4.152E-11	5.114E-11	-1.727E-13	3.594E-14	100	2.599E+03	1.653E+02	2058.0	78.6	0	0	401
1300	1	4.895E-09	1.197E-10	1.592E-12	4.524E-14	9.598E-13	3.311E-14	-2.998E-11	4.636E-11	1.452E-13	3.411E-14	99.912	3.047E+03	9.333E+01	2258.1	40.6	0	0	401
TOTAL		2.442E-08	4.197E-10	1.042E-11	2.106E-13	5.887E-12	1.419E-13	1.652E-10	1.470E-10	5.454E-13	1.132E-13	99.4	2.370E+03	5.312E+01	1946.8	28.1	16.134	14.612	
Typical BLANK		2.208E-12	5.234E-13	2.241E-13	2.650E-14	2.845E-13	1.814E-14	1.930E-13	1.440E-14	5.704E-13	2.310E-14								
Plateau Age (806°C−1038°C, 62.7% of ^{39}Ar released):															1838	31			

(^{40}Ar/^{36}Ar)$_{Air}$	296	Nier (1950)
(^{38}Ar/^{39}Ar)$_{Air}$	0.188	Nier (1950)
(^{40}Ar/^{39}Ar)$_{K}$	(3.478 ± 0.254)E-1	(measured) *4
(^{39}Ar/^{37}Ar)$_{Ca}$	(1.098 ± 0.261)E-3	(measured)
(^{36}Ar/^{37}Ar)$_{Ca}$	(3.185 ± 1.126)E-4	(measured)

Decay Constants

^{40}K λ_e	5.81E-11 a^{-1}	Steiger and Jager (1977)
^{40}K λ_β	4.692E-10 a^{-1}	Steiger and Jager (1977)
^{39}Ar	258 a^{-1}	Walker etal. (1989)
^{37}Ar	0.0665 a^{-1}	Walker etal. (1989)

*1: Errors are shown in 2 sigma.
*2: ^{37}Ar is corrected for decay
*3: Temperature was incorrect due to emissivity change, but the power is higher than the previous step.
*4: No cadmium shield

Table 2. Paleomagnetic results

	n	Dec	Inc	k	α_{95}
GP72 (HT)	9	242.4	67.4	66.9	6.3
GP75 (HC)	8	245.0	65.1	113.0	5.2
Mean	17	243.6	66.3	83.4	3.9

HT, High temperature component; HC, High coercivity component.

Table 3. Paleointensitiy results

Sample	TR(℃)	n	slope	β	f	g	q	MAD anchored	α	δ（CK）	δ(t*)	δ(TR)	F	ΔF
GP720111	440-560	8	-1.07	0.09	0.37	0.84	3.5	5.8	14.7	3.7	1.4	1.9	16.02	1.42
GP720113	400-550	8	-0.87	0.07	0.34	0.83	4.1	3.9	8.5	1.7	2.0	1.2	13.00	0.90
GP720712	400-551	8	-1.09	0.13	0.32	0.83	2.1	3.1	6.9	2.5	1.7	2.3	16.31	2.11
GP720212	400-552	8	-1.00	0.08	0.32	0.82	3.1	2.8	6.4	2.6	1.4	1.1	15.03	1.27
GP721531	400-553	8	-1.27	0.15	0.32	0.81	1.7	4.3	9.3	4.2	2.6	1.4	18.98	2.93
GP721221	350-560	9	-1.25	0.15	0.55	0.85	3.2	6.4	13.0	4.8	4.1	5.8	18.72	2.74
GP720121	450-560	8	-0.84	0.11	0.41	0.81	2.9	5.9	14.7	1.8	1.3	0.6	12.66	1.43
GP720131	450-560	8	-0.77	0.1	0.38	0.81	3.1	5.8	14.9	1.4	0.9	0.5	11.51	1.15
GP720312	350-560	10	-0.97	0.11	0.37	0.86	3.0	5.6	13.4	3.8	0.9	0.9	14.51	1.56
GP720541	350-561	10	-1.06	0.13	0.42	0.86	2.9	5.0	13.4	2.3	0.9	2.6	15.84	1.99
GP721021	400-560	9	-0.92	0.11	0.46	0.78	3.1	6.8	7.2	3.9	0.9	1.1	13.83	1.59
GP721022	350-560	10	-0.8	0.1	0.41	0.85	3.4	5.6	14.1	4.7	1.2	1	11.95	1.24
GP721521	350-560	10	-0.96	0.09	0.51	0.82	4.8	6.4	12.8	2.7	1.7	1.2	14.44	1.27

Notes: TR, temperature range for the linear segment; n, number of data point included in the linear regression; slope, slope of the segment; β, the standard error of the slope divided by the slope itself;f,g,q, quality parameters after Coe et al.(1978); MAD, quality parameter of the linearity after Kirschvink (1980); α, angular difference between anchored to the origin and non-anchored direction; δ(CK); pTRM check parameter; δ(t*),δ(TR), parameters relate to the pTRM tail check (Leonhardt et al., 2004) ; F, ΔF, paleointensity and its standard deviation.

Table 4 Paleomagnetic directions from Nuuk area in Greenland

	n	Dec	Inc	k	α95	VGP Lat	VGP Long	VGP(rotated) Lat	VGP(rotated) Long	Age	Reference
Proterozoic dykes											
GP1	13	255.4	74.6		4.7	47.3	-95.3	45.6	-101.6	2752±63 (K-Ar plagioclase)	Morimoto et al., 1997
GP8	24	253.0	62.6	229.6	2.5	32.2	-106.2	31.4	-114.3	2585±21 (Ar-Ar pyroxene)	Miki et al., 2009
GP7	17	243.6	66.3	83.4	3.4	33.5	-96.4	31.9	-104.5	1816±15 (Ar-Ar clinopyroxene)	This study
Archean Gneiss											
GP1		225.9	55.2		4.8	16.2	-89.1				Morimoto et al., 1997
GP8	16	224.6	64.6	239.7	2.4	26	-84.3				Miki et al., 2009
F&B	8	225	60	57	7.5	20.9	-86.6				Fahrig & Bridgewater, 1976

VGPs(rotated) are rotated by 12°back to North America about the Euler pole of 66.6°N, 119.5°W (Roest and Srivastava, 1989), in order to indicate the positions before the Cretaceous Labrador Sea opening.

Table 5 Paleomagnetic directions from Nagssugtoqidian fold belt

						VGP				VGP (Rotated)				
		Dec	Inc	k	α 95	Lat	Long	dp	dm	Lat	Long			
Metamorophosed dykes and gneiss														
N Strom Gneiss	4	222.3	56.4	67	11.3	19.3	272.2	11.8	16.3	17.1	-97.4			Beckmann 2013
Morgan Dyke+gneiss	22	207.1	54.2	46	4.6	13.4	283.9	4.6	6.5	10.5	-86.3			Morgan 1976
Piper Alt	24	213.0	67.8	34	5.2	30.1	283.9	7.2	8.7	27.1	-85.1			Piper 1981
Piper It	38	198.8	59.1	25	4.8	17.5	291.7	5.3	7.1	14.1	-78.4			Piper 1985
Mean	4									17.3	273.2	k=61.1	α95=11.8	
Unmetamorophosed dykes														
Kangamiut Dyke	22	220.3	56.6	225	2.1	17.7	273.8	2.2	3	15.4	-96			Fahrig & Bridgewater 1976

VGPs(rotated) are rotated by 12° back to North America about the Euler pole of 66.6°N, 119.5°W (Roest and Srivastava, 1989), in order to indicate the positions before the Cretaceous Labrador Sea opening.

Figure 1.

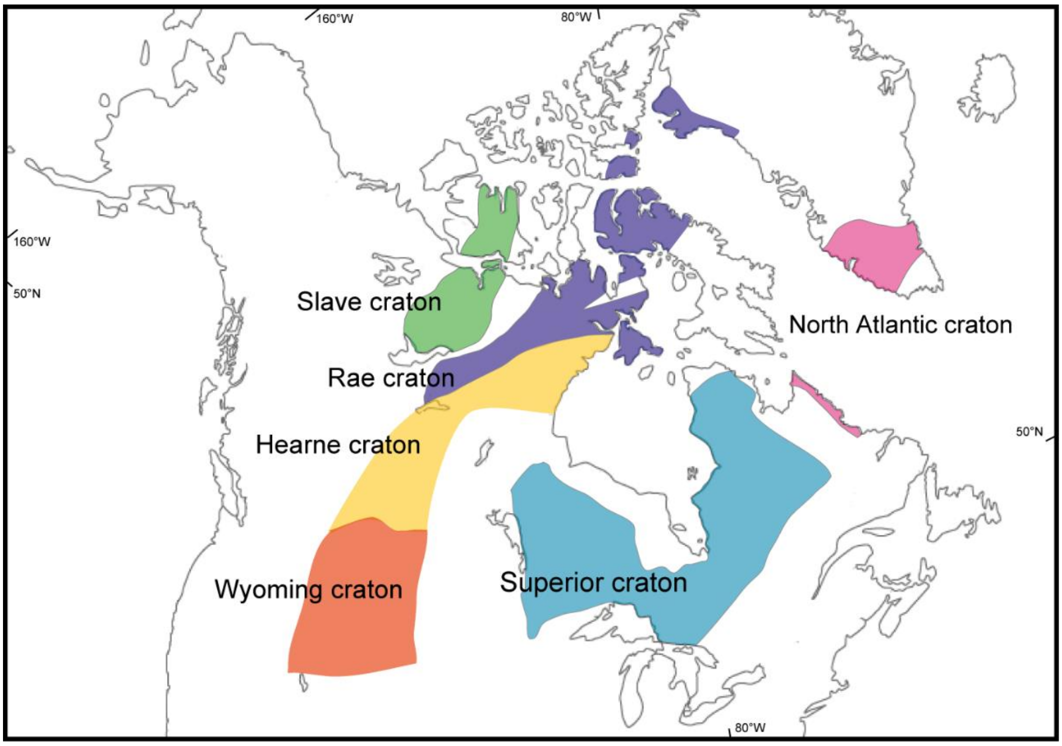

Fig. 1 Archean cratons of Laurentia. Modified from Mitchell et al. (2014).

Figure 2.

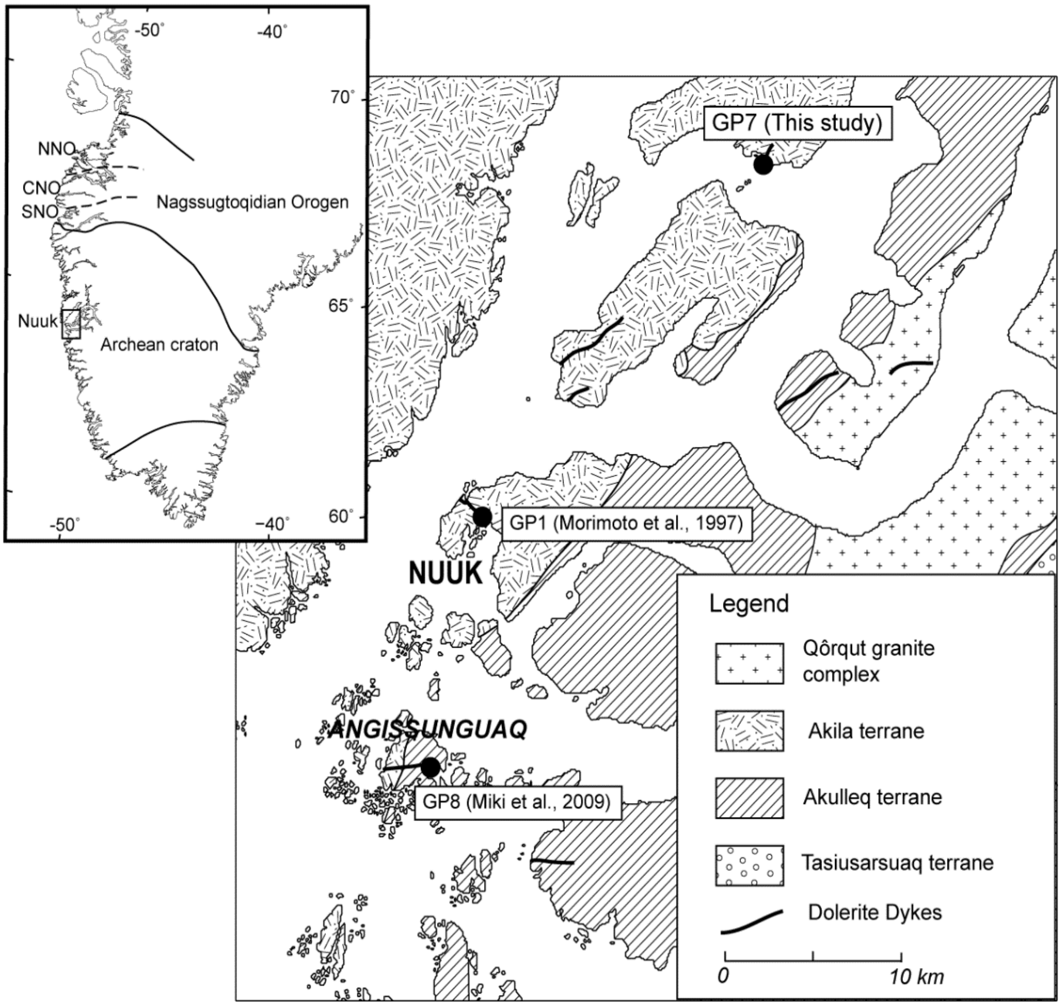

Fig. 2. Simplified tectonic and geological maps of southern Greenland with sampling localities. NNO, CNO, and SNO; Northern, Central, and Southern Nagssugtoqidian orogeny, respectively. Geological map is after Friend et al. (1996).

Figure 3.

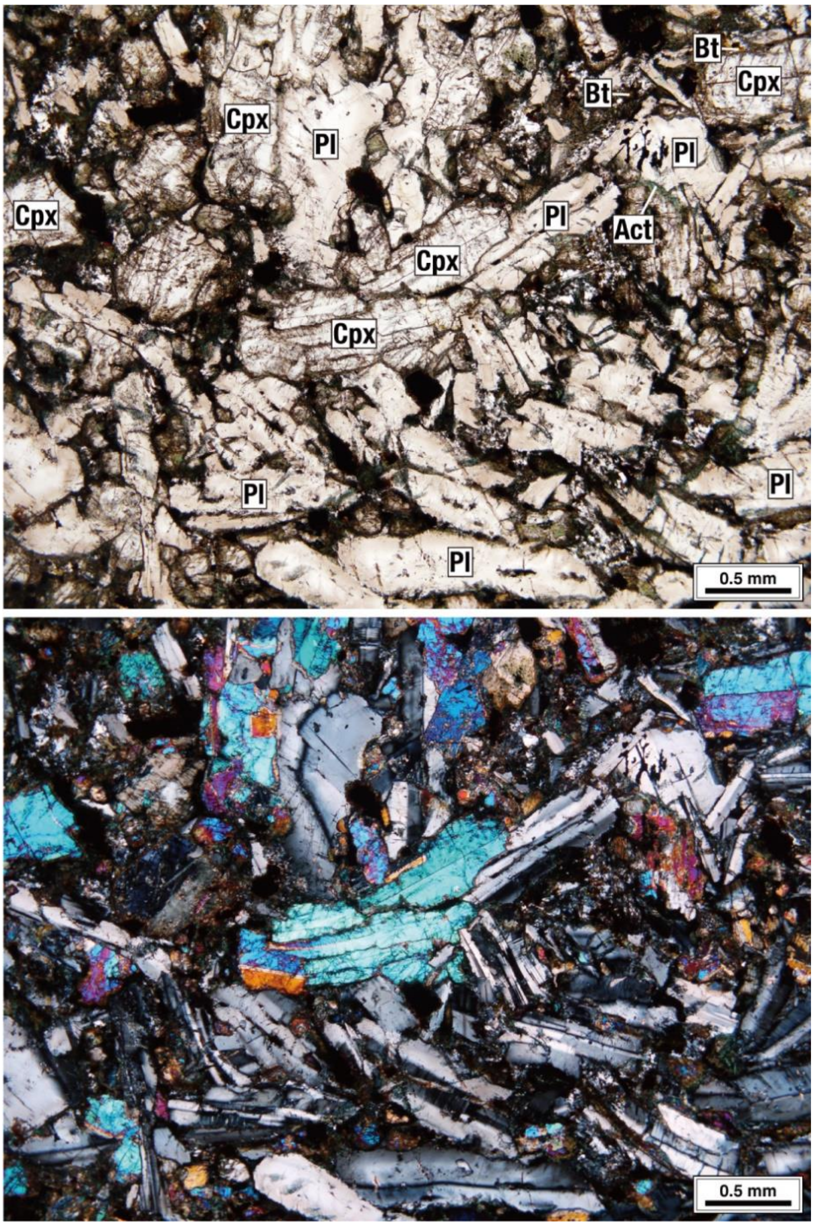

Fig. 3. Microscopic images of the dolerite: (a) Plane-polarized light image and (b) cross-polarized light image.

Figure 4

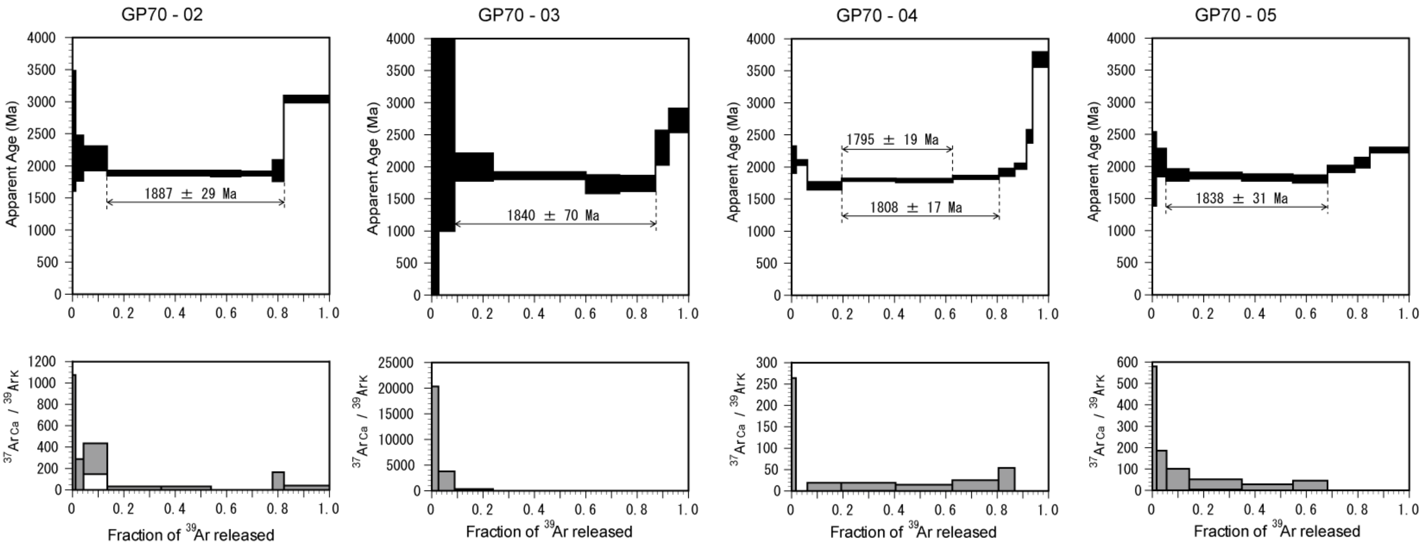

Fig.4. $^{40}Ar/^{39}Ar$ age spectra and $^{37}Ar_{Ca}/^{39}Ar_{K}$ ratios for clinopyroxene crystals using step-heating analyses. Lines with arrows denote plateau steps used in age calculations.

Figure 5

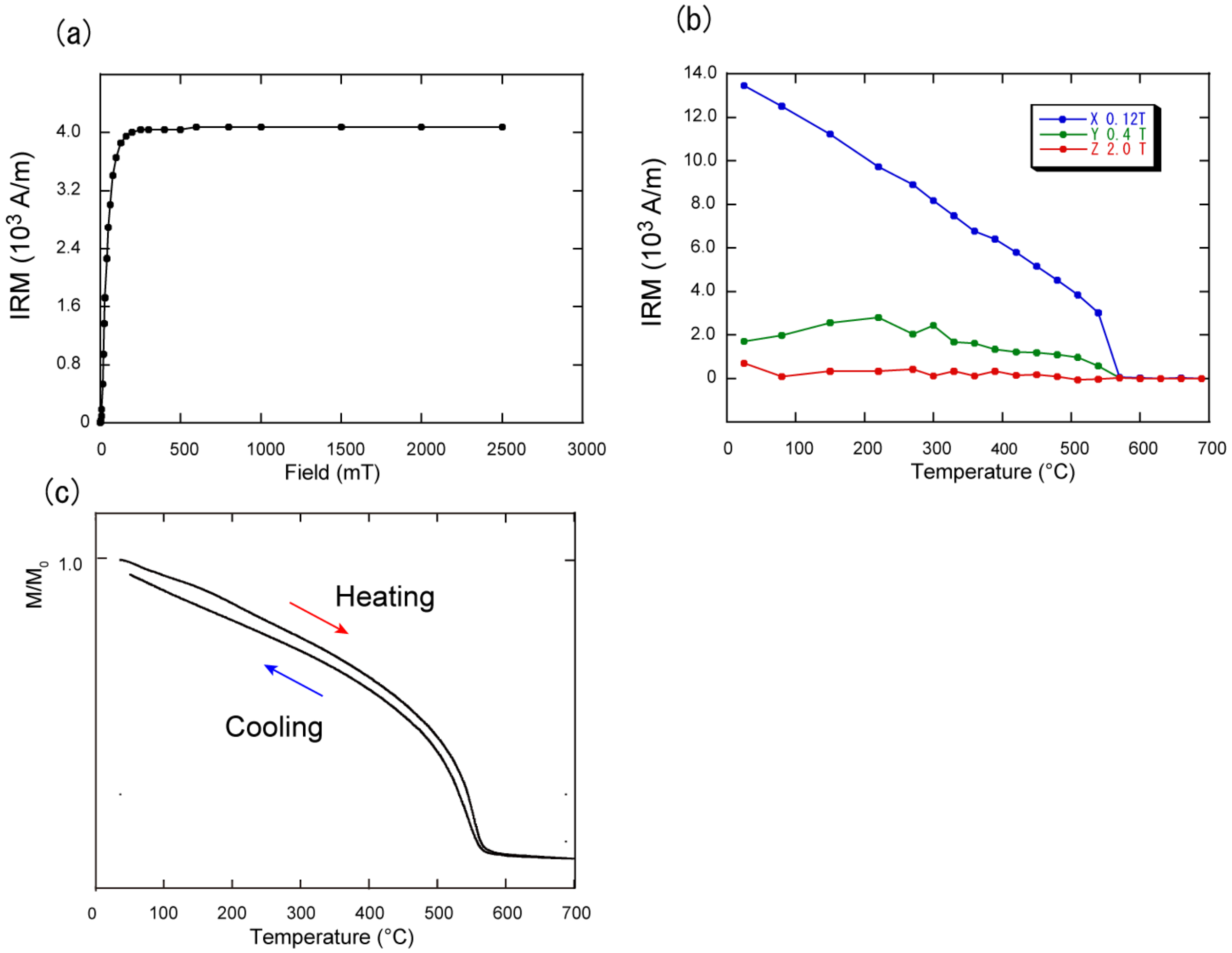

Fig. 5. Typical results of rock magnetic experiments. (a) Stepwise IRM acquisition experiments; (b) thermal demagnetization of the composite IRMs acquired along three perpendicular axes; and (c) high-field thermomagnetic analyses.

Figure 6.

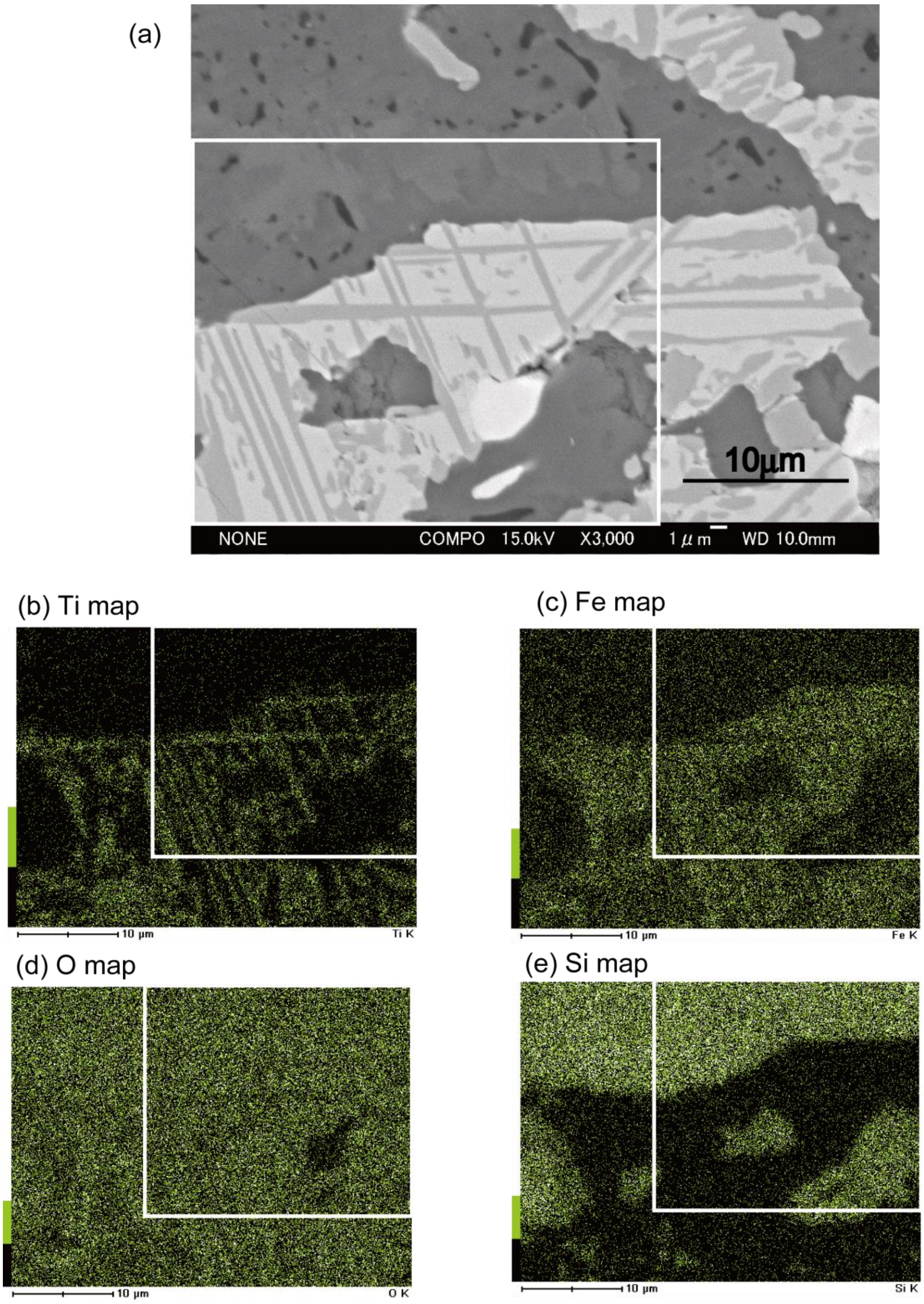

Fig. 6. (a) SEM backscattering image of the dolerite dyke sample. (b)–(d) Elemental mapping images of the area indicated by the thick rectangular in (a).

Figure 7

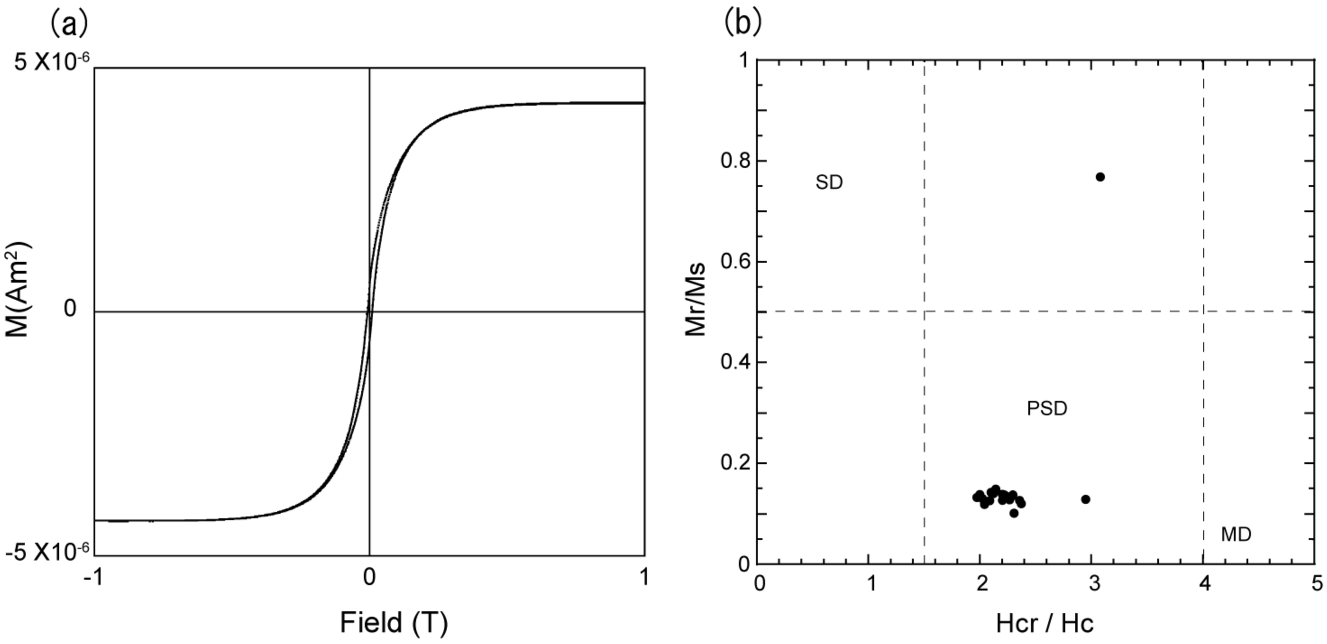

Fig. 7. (a) A typical hysteresis curve for dolerite specimen. (b) Hysteresis parameters on the Day plot.

Figure 8

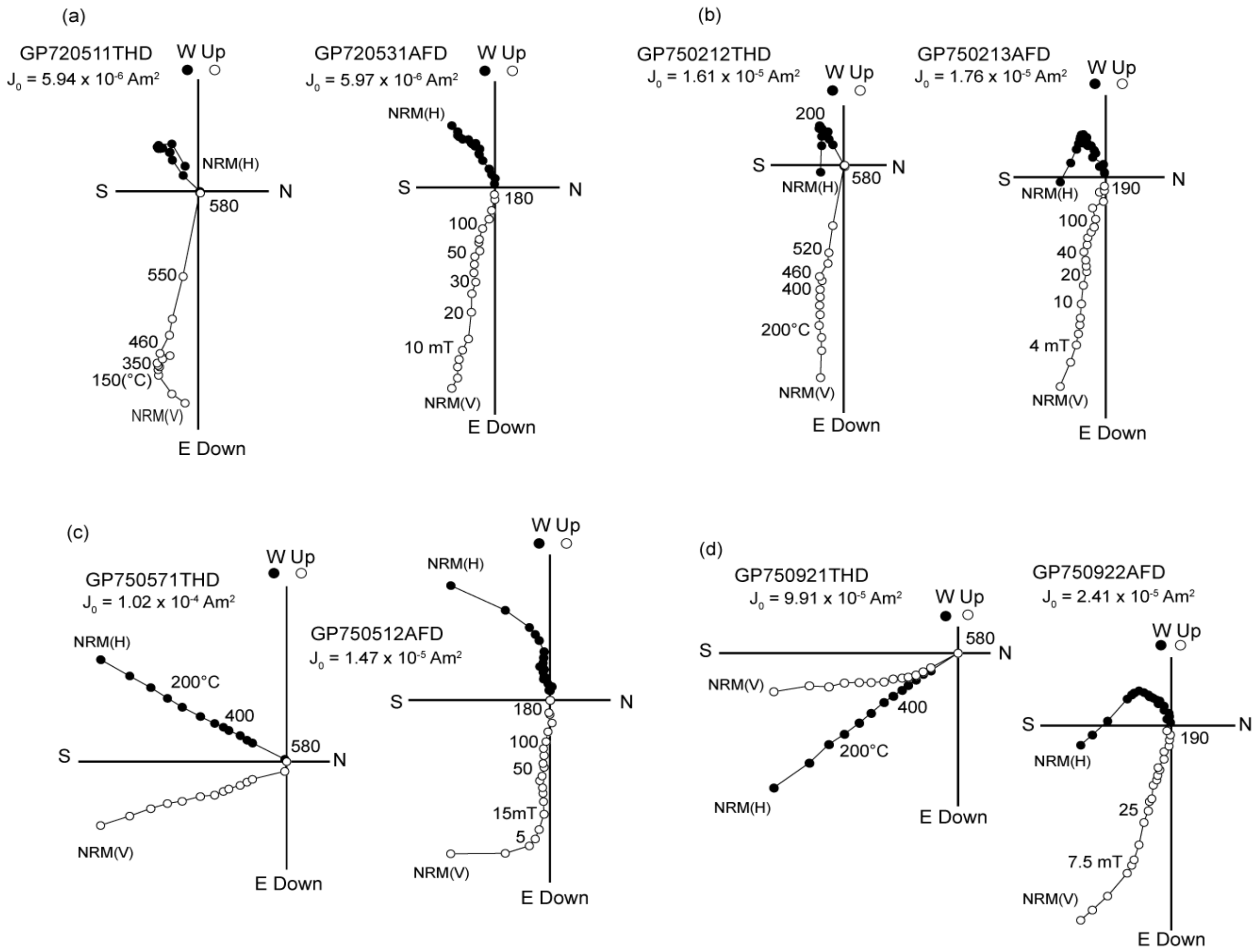

Fig. 8. The orthogonal plots of stepwise thermal demagnetization experiments for dolerite dyke specimens. (a) Results from the eastern margin (GP72); (b), (c), and (d) results from the western margin (GP75). The behavior of the specimens from GP75 is different between those of thermal demagnetization (THD) and alternating-field demagnetization (AFD).

Figure 9

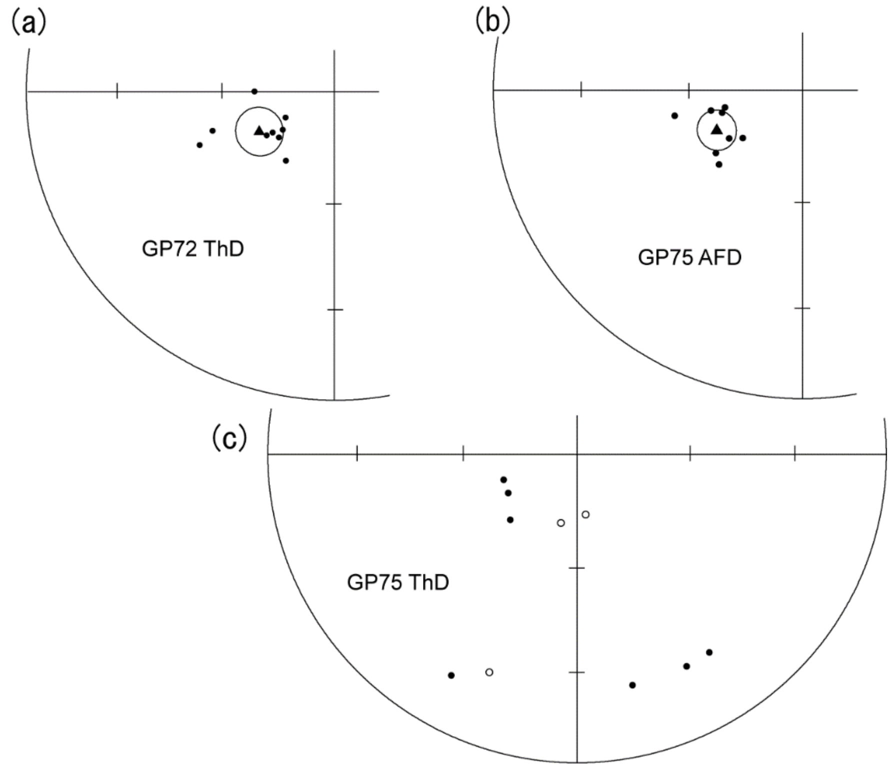

Fig. 9. Comparison of high-temperature components and high-coercivity components between GP72 and GP75. (a) High-temperature components from GP72; (b) high-coercivity components from GP75; and (c) high-temperature components from GP75.

Figure 10

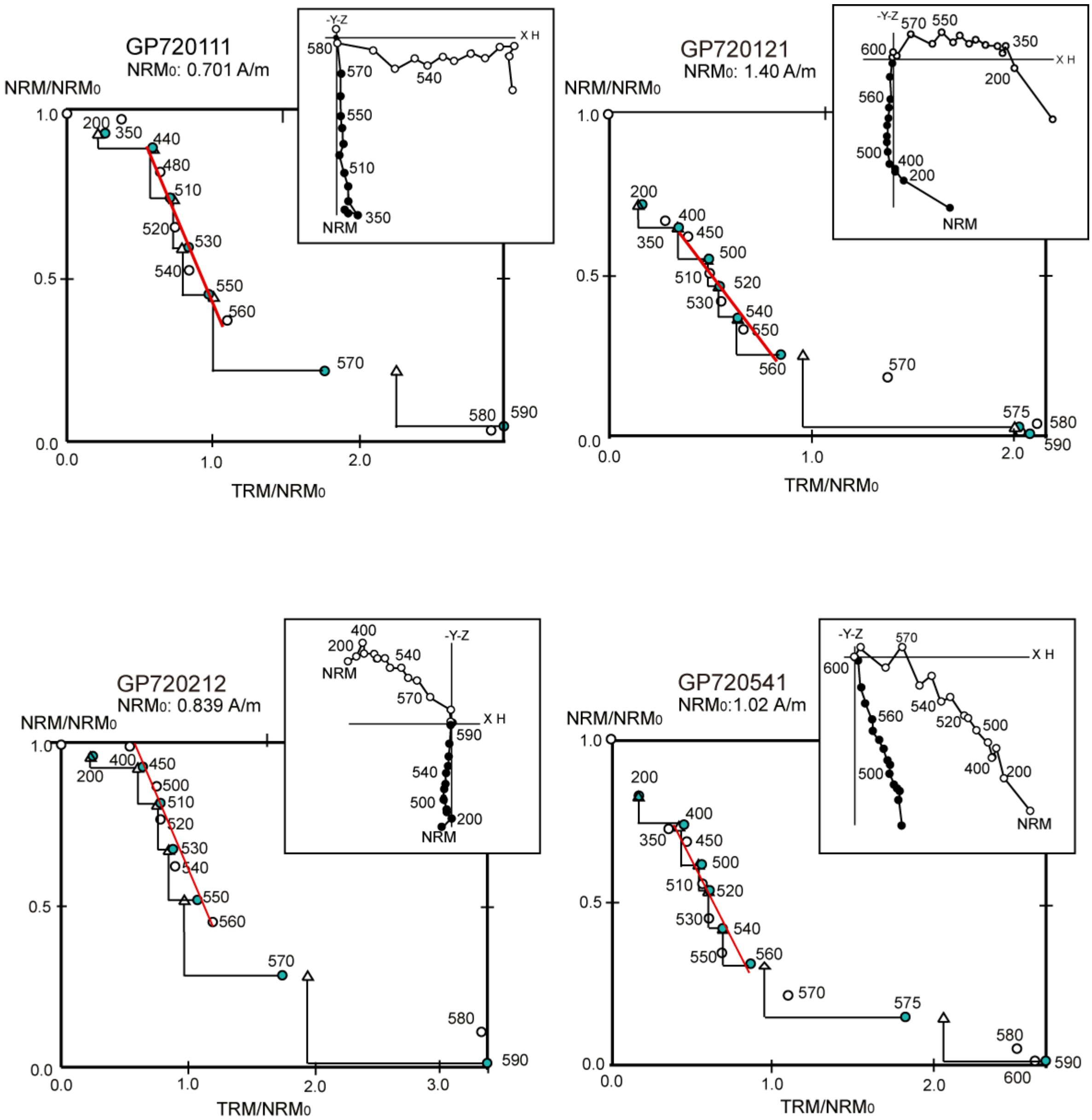

Fig. 10. Representative results from the Thellier experiments. In the NRM–TRM diagrams (Arai plots), open (solid) symbols indicate IZ (ZI) protocols. NRM and TRM are normalized by the initial NRM (NRM_0). Triangles are the pTRM check steps. In orthogonal vector plots, the open (solid) symbols indicate projections on horizontal (vertical) planes.

Figure 11

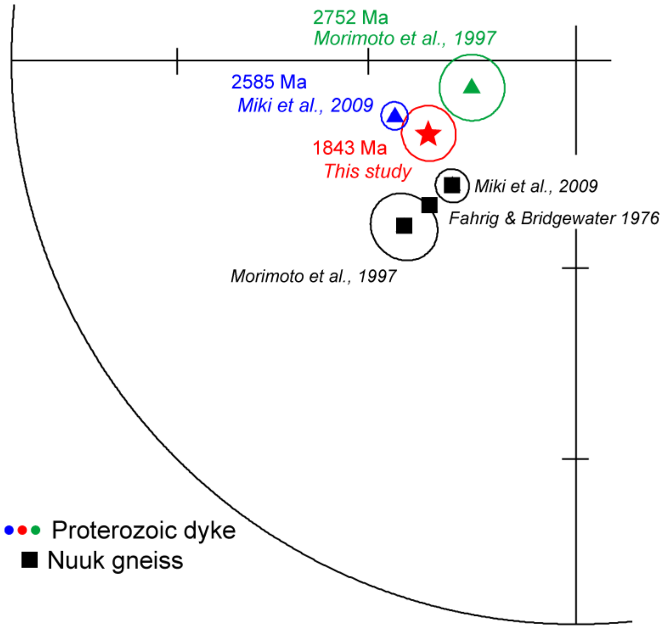

Fig.11. Paleomagnetic directions of Proterozoic dykes and Archean gneiss in Nuuk area with α_{95} confidence circles. Equal area projections.

Figure 12

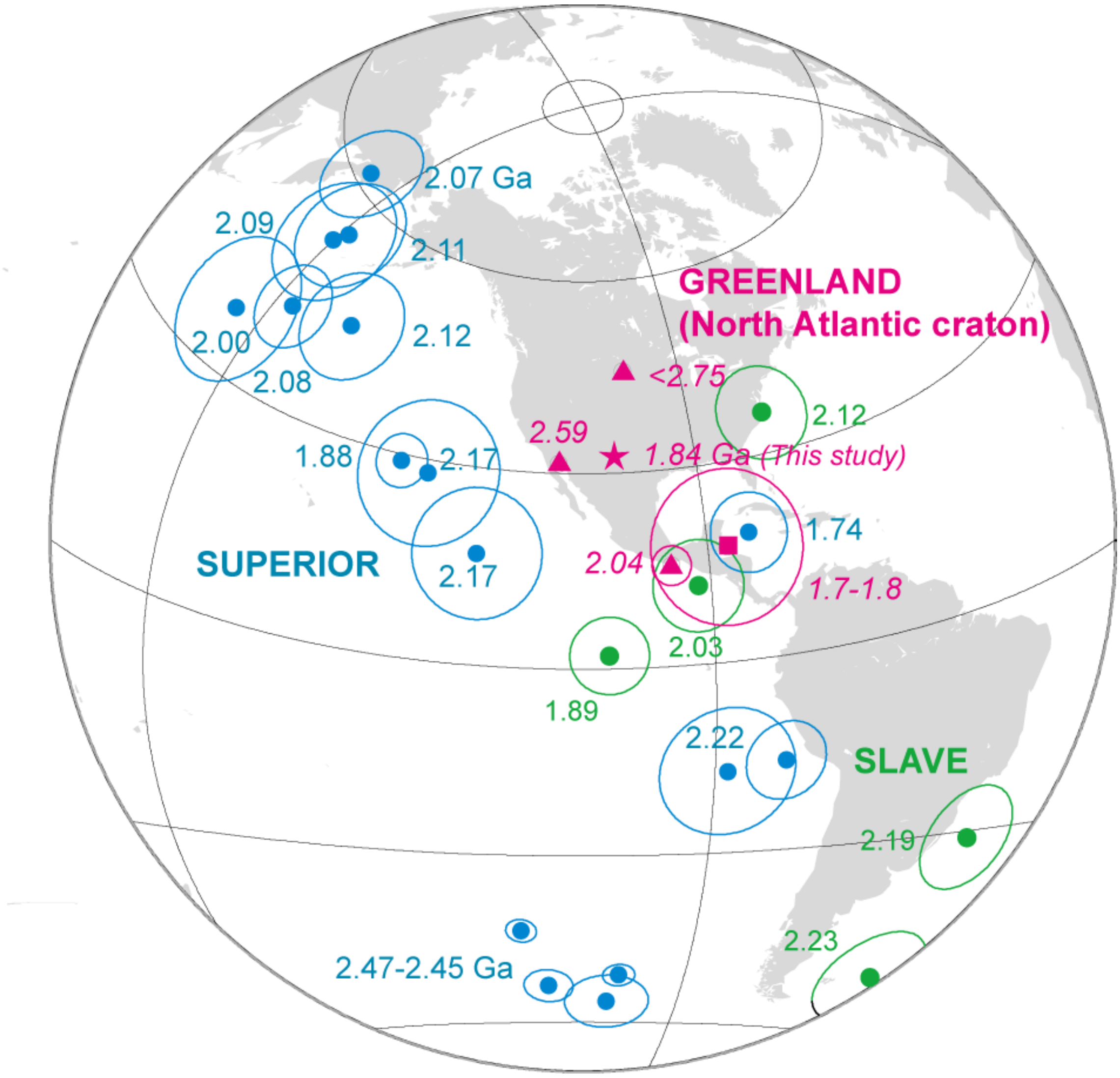

Fig.12. Paleoproterozoic paleomagnetic poles from southern West Greenland (red) and these from the Superior (blue) and Slave (green) Cratons of North America. The Greenland poles (red symbols) are rotated by 12° back to North America about the Euler pole of 66.6°N, 119.5°W (Roest and Srivastava, 1989) in order to indicate the VGP positions before the Cretaceous Labrador Sea opening between North America and Greenland. The key poles of Slave (green circles) and Superior (blue circles) Cratons are from Buchan (2013) and Buchan et al. (2016).

Figure 13

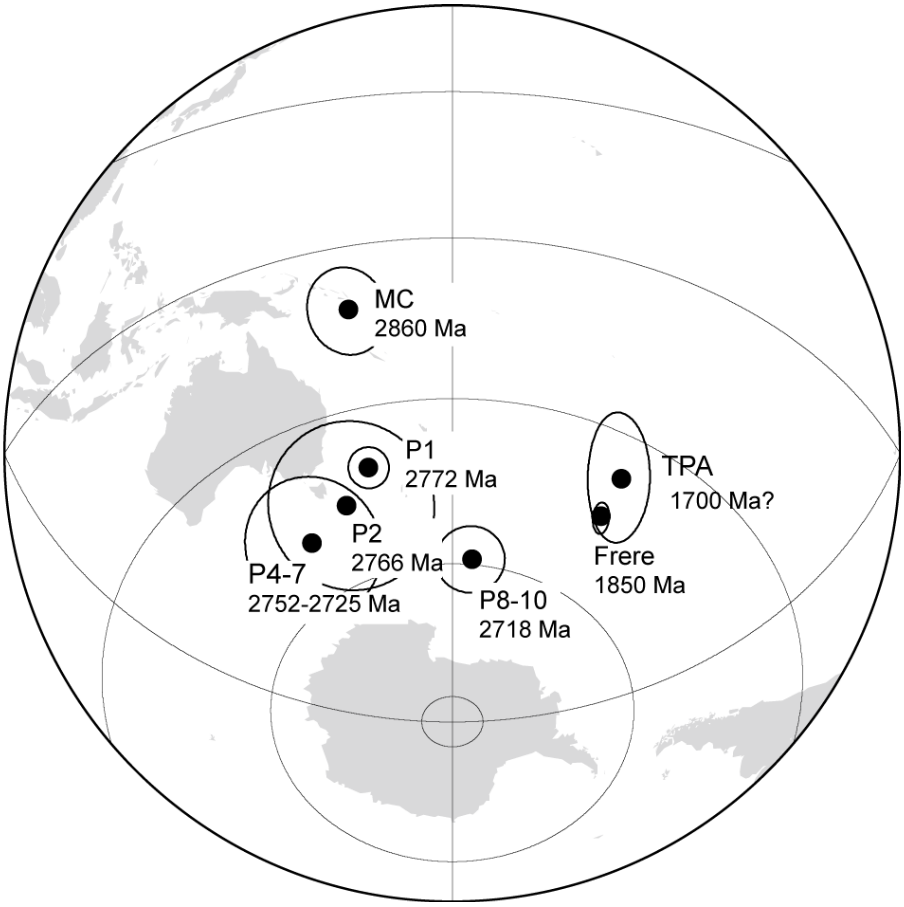

Fig.13. Paleoproterozoic poles from the Pilbara Craton in Australia. Poles are MC (Millimdinna Complex, Schmidt and Embleton, 1985); P1, P2, P4-7, P8-10 (Pilbara Flood Basalts, Strik et al., 2003), Frere (Frere Formation, Williams et al., 2004), and TPA (Mt. Yom Price Iron Ore, Schmidt and Clark, 1994).

Figure 14

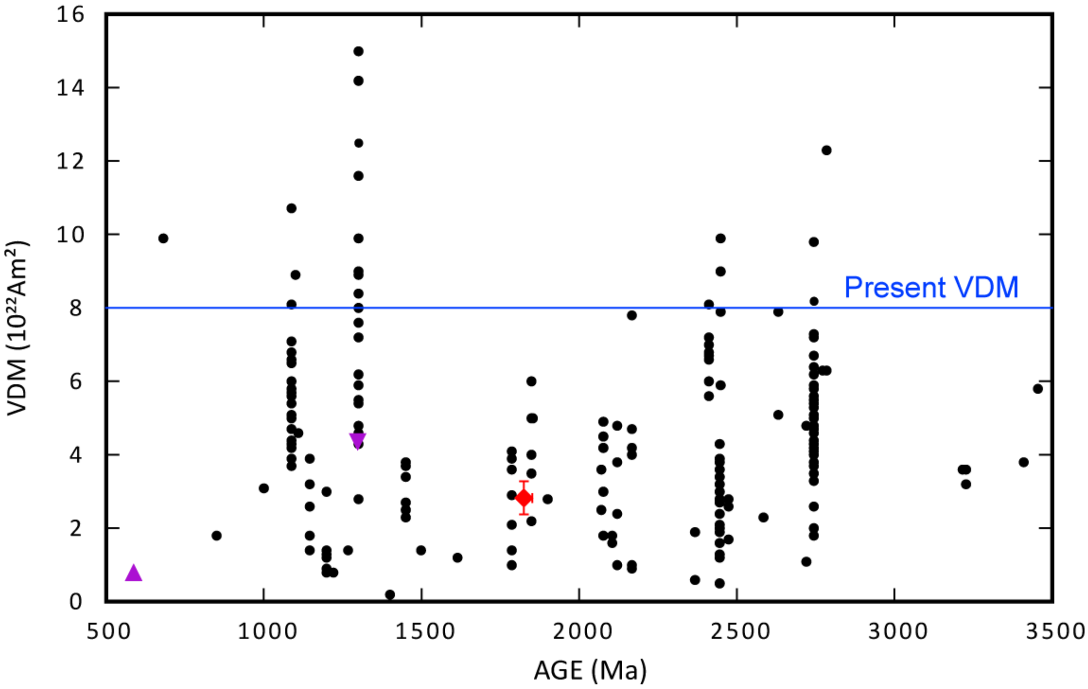

Fig. 14. Comparison of Precambrian VDMs from this study and that from the global database of PINT 2015 (Veikkolainen et al., 2017). The data with Qpi >= 3 are chosen (Biggin & Peterson, 2014). The red symbol is the data for this study. Two recent VDM data are also plotted (the purple upward triangle, Bono et al., 2019; the purple downward triangle, Kodama et al., 2019). The blue line represents the present dipole moment value of ~8.0 × 10^{22} Am^2.10^{-12} ccSTP, respectively.